Journal of Medicinal Chemistry

pubs.acs.org/jmc

Article

Phenolic Lipids Derived from Cashew Nut Shell Liquid to Treat Metabolic Diseases

Cigdem Sahin,[○] Lilia Magomedova,[○] Thais A. M. Ferreira,[○] Jiabao Liu, Jens Tiefenbach, Priscilla S. Alves, Fellipe J. G. Queiroz, Andressa S. de Oliveira, Mousumi Bhattacharyya, Julie Grouleff, Patrícia C. N. Nogueira, Edilberto R. Silveira, Daniel C. Moreira, José Roberto Souza de Almeida Leite, Guilherme D. Brand, David Uehling, Gennady Poda, Henry Krause, Carolyn L. Cummins,*[,⊗] and Luiz A. S. Romeiro*[,⊗]

Cite This: *J. Med. Chem.* 2022, 65, 1961−1978

Read Online

ACCESS | Metrics & More | Article Recommendations | Supporting Information

ABSTRACT: Metabolic diseases are increasing at staggering rates globally. The peroxisome proliferator-activated receptors (PPAR$\alpha/\gamma/\delta$) are fatty acid sensors that help mitigate imbalances between energy uptake and utilization. Herein, we report compounds derived from phenolic lipids present in cashew nut shell liquid (CNSL), an abundant waste byproduct, in an effort to create effective, accessible, and sustainable drugs. Derivatives of anacardic acid and cardanol were tested for PPAR activity in HEK293 cell co-transfection assays, primary hepatocytes, and 3T3-L1 adipocytes. *In vivo* studies using PPAR-expressing zebrafish embryos identified CNSL derivatives with varying tissue-specific activities. LDT409 (**23**) is an analogue of cardanol with partial agonist activity for PPARα and PPARγ. Pharmacokinetic profiling showed that **23** is orally bioavailable with a half-life of 4 h in mice. CNSL derivatives represent a sustainable source of selective PPAR modulators with balanced intermediate affinities (EC_{50} ∼ 100 nM to 10 μM) that provide distinct and favorable gene activation profiles for the treatment of diabetes and obesity.

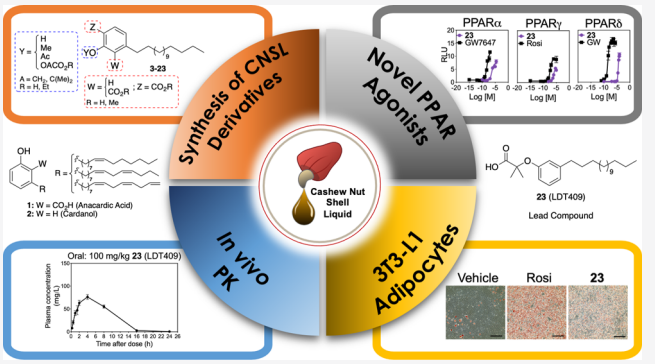

INTRODUCTION

Metabolic syndrome refers to a constellation of medical conditions that include elevated fasting glucose levels, hypertension, high triglyceride levels, abnormal cholesterol profiles, and excess abdominal fat.[1] Metabolic syndrome is a major global health concern affecting ∼25% of adults worldwide[2] and increasing the risk of type 2 diabetes, cardiovascular disease, and death.[3−6] Pharmacological targeting of the peroxisome proliferator-activated receptor (PPAR) subclass of nuclear receptor proteins has been used to combat metabolic disease.[7−9]

The PPARs are transcription factors that act as heterodimers with the retinoid X receptor (RXR) and bind directly to DNA. Upon ligand activation, there is a conformational change in the receptor that promotes interaction with co-regulators, thereby modulating the recruitment of basal transcriptional machinery and influencing gene expression.[10,11] Importantly, the PPARs are activated by endogenous ligands (fatty acids, lipid metabolites, and eicosanoids) at micromolar concentrations and synthetic ligands at nanomolar concentrations.[12,13] There are three isoforms: PPARα, PPARγ, and PPARδ.[14] PPARα is predominantly expressed in the liver and coordinately regulates the transcription of genes important in liver fatty acid uptake and fatty acid utilization, thereby decreasing plasma triglycerides.[15] In contrast, PPARγ is most highly expressed in adipose tissue and serves to enhance insulin sensitivity and regulate adipogenesis.[16] PPARδ is ubiquitously expressed including the small intestine, liver, brain, and skeletal muscle. Activation of PPARδ in skeletal muscle improves insulin sensitivity and enhances energy utilization as well as endurance exercise capacity.[17,18] These properties make each PPAR receptor unique in its regulation of lipid metabolism and glucose homeostasis.[19]

Antihyperlipidemic agents, known as the fibrate class of drugs (gemfibrozil, clofibrate, fenofibrate, bezafibrate) (Figure 1), target PPARα and are effective at lowering hypertriglyceridemia and increasing high-density lipoprotein choles-

Received: August 30, 2021
Published: January 28, 2022

https://doi.org/10.1021/acs.jmedchem.1c01542
J. Med. Chem. 2022, 65, 1961−1978

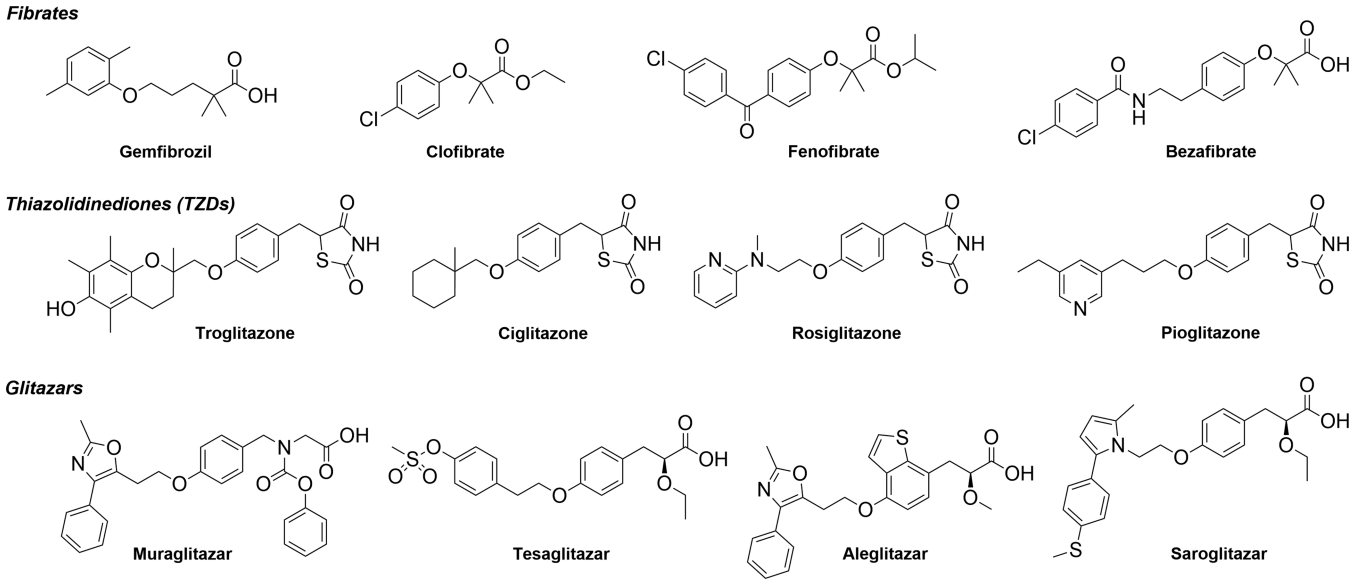

Figure 1. Chemical structures of fibrates, thiazolidinediones (TZDs), and glitazars.

terol (HDL-C).[20] The insulin-sensitizing thiazolidinedione (TZDs) drugs (troglitazone, ciglitazone, rosiglitazone, pioglitazone) (Figure 1) target PPARγ and are used to improve insulin sensitivity in patients with type 2 diabetes.[8,16] The glitazars (muraglitazar, tesaglitazar, aleglitazar, saroglitazar) (Figure 1) target PPARα and PPARγ and were developed to simultaneously treat hyperlipidemia and hyperglycemia. However, prolonged use of TZDs and glitazars lead to major PPARγ-related side effects including congestive heart failure, weight gain, bone loss, and edema, thus severely limiting their use and/or halting their further development.[16,19,21,22] These side effects are specifically related to the high affinity, full agonistic activity, and potency of these compounds on the PPARγ receptor.[16,19,21]

A drug that combines the best features of both PPARα and PPARγ activation with an improved safety profile would be an attractive therapeutic modality for the treatment of metabolic syndrome, type 2 diabetes, and hyperlipidemia.[23,24] Partial PPARγ agonists or weak PPARγ ligands have previously been shown in mice to have insulin-sensitizing effects without the side effect of weight gain.[25−27] Compounds with these characteristics are termed selective PPAR modulators (SPPARMs) and are characterized by their tissue-selective and/or gene-selective activities.[21,28] A key feature of SPPARMs is their ability to allow the separation of the negative effects of PPAR activation from the beneficial (therapeutic) effects.

Based on the above considerations, we have been exploring the phenolic lipids of cashew nut shell liquid (CNSL), an inexpensive and widely available starting material, for developing new low-cost and sustainable drugs.[29−32] These natural compounds have privileged structures capable of mimicking fatty acids and act as signaling molecules that regulate various physiological effects on metabolism and inflammation.[33−36] Herein, we developed novel PPAR agonists with properties similar to endogenous ligands in that they have balanced affinities and/or partial agonist activity for PPARα and PPARγ. This work was inspired by the structural similarity between fatty acids, which function as endogenous ligands of PPARs, and anacardic acid (**1**) and cardanol (**2**) mixtures—the main phenolic compounds of the natural and technical-grade cashew nut shell liquid of *Anacardium occidentale*, respectively.[37] Figure 2 shows the structural similarity of stearic acid with saturated anacardic acid.

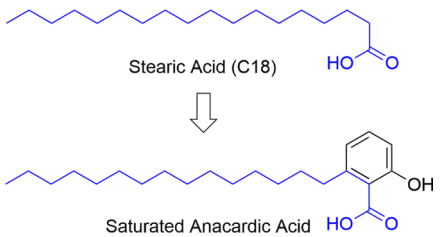

Figure 2. Similarity of chemical structures of stearic acid and saturated anacardic acid.

RESULTS AND DISCUSSION

Chemical Design. A new series of saturated anacardic acid derivatives were designed to identify structural features relevant for PPAR receptor recognition. To create molecular diversity and to delineate preliminary structure−activity relationships (SAR), cardanol was included as it is another major component of technical-grade CNSL. Our purpose was to determine whether these novel compounds derived from this natural resource could serve as SPPARMs with eventual application for the treatment of metabolic disease. Toward this goal, we turned our attention to scaffolds that share a C15 saturated alkyl chain as a basic feature of the fatty acid mimetics, in this case, sustainable and cost-effective for drug development.[38] Also, the presence of an acid group completes the structural requirements for molecular recognition by PPAR. Thus, we designed derivatives of anacardic (6-pentadecyl-2-hydroxybenzoic) and isoanacardic (4-pentadecyl-2-hydroxybenzoic) acids with O-substitutions in the phenol to obtain O-acetylated and O-methylated derivatives. For the cardanol series (3-pentadecylphenol and (*Z*)-(3-pentadec-8-en-1-yl)phenol), the same O-variations designed for the acids were planned. To overcome the absence of the carboxylic group in cardanol, α-phenoxyalkyl acid derivatives were designed through the insertion of the carboxymethylene

https://doi.org/10.1021/acs.jmedchem.1c01542
J. Med. Chem. 2022, 65, 1961−1978

subunit including its analogue with the geminal dimethyl group found in some fibrates (Figure 1). The design strategy of CNSL derivatives is shown in Figure 3.

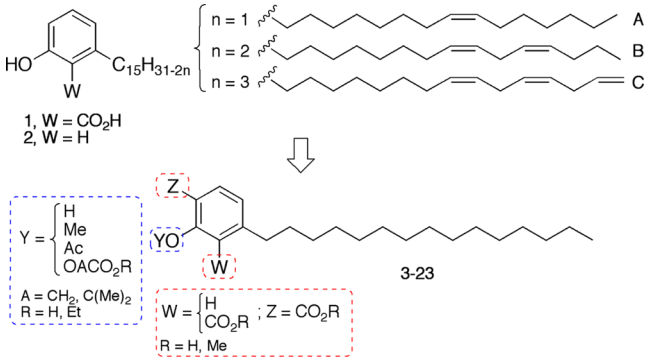

Figure 3. Saturated derivatives (**3**−**23**) designed from the mixtures of anacardic acids (**1**) and cardanols (**2**).

Chemistry. Overall, 25 compounds (**3**−**27**) were synthesized following the routes outlined in Schemes 1−3. Isolations

Scheme 1. Synthesis of Anacardic Acid Derivatives 3−8[a]

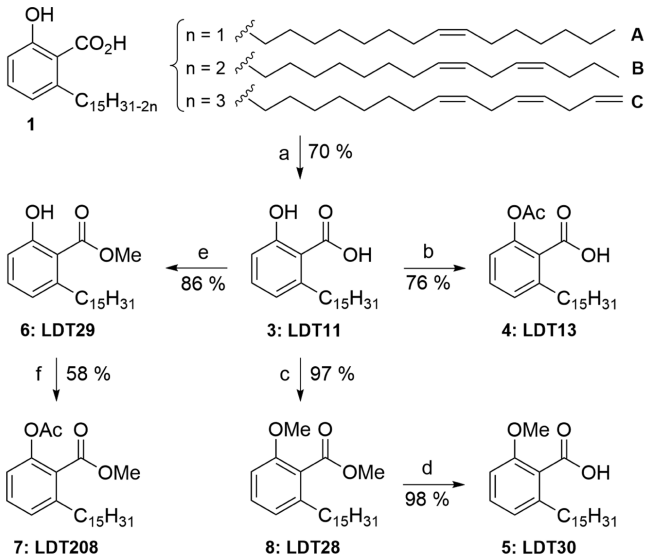

[a]Reagents and conditions: (a) H_2, Pd/C 10%, EtOH, room temperature (r.t.), 6 h; (b) AC_2O, H_3PO_4, microwave (MW), 3 min; (c) MeI, K_2CO_3, Me_2CO, 120 °C, 16 h; (d) *t*-BuOK, DMSO, 40 °C, 16 h; (e) MeOH, H_2SO_4, 50 °C, 16 h; (f) AcCl, TEA, CH_2Cl_2, r.t. 16 h.

of the anacardic acids (**1**) and cardanol (**2**) mixtures, respectively, obtained from natural and technical CNSL, were performed according to Rossi et al.[31] To synthesize derivatives **4**−**8**, we started with the hydrogenation of the unsaturated chains present in the mixture **1** using Pd/C 10% as catalyst in a Parr hydrogenation apparatus to obtain the saturated anacardic acid (**3**). Then, **3** was O-acetylated with acetic anhydride and H_3PO_4 to give the acetoxy-derivative **4**. Taking advantage of the differential reactivity of the phenol and carboxylic acid groups, obtaining acid **5** with methylated phenolic hydroxyl was carried out in two steps. First, **3** was converted to the derivative O,O-dimethylated **8** with methyl iodide in acetone at 102 °C using condenser cooling to −8 °C. Next, the methyl ester **8** was hydrolyzed with *t*-BuOK in dimethyl sulfoxide (DMSO) at 40 °C leading to derivative **5**. To synthesize derivatives **6** and **7**, the acid **3** was transformed into the corresponding methyl salicylate **6** by the Fischer reaction in methanol catalyzed with H_2SO_4 and the ester was converted to the *O*-acetyl derivative **7** with acetyl chloride/triethylamine (TEA) in dichloromethane (Scheme 1).

The derivatives **12**−**23** have as the precursor the saturated cardanol **9** obtained by the catalytic hydrogenation of mixture **2** with Pd/C 10% in ethanol. To synthesize compounds **12**−**17** (isoanacardic acid series), **9** was transformed into salicylaldehyde **10** by regiospecific ortho-formylation with paraformaldehyde, $MgBr_2$, and triethylamine in THF under reflux. Then, **10** was converted to the methoxy-derivative **11** with methyl iodide at 65 °C. Both aldehydes **10** and **11** were oxidized with $NaClO_2$ in the presence of NaH_2PO_4 in a mixture DMSO/CH_2Cl_2 (1:1), providing the respective acids **12** and **14**. In turn, the acids were converted to the methyl esters **15** and **17** with methanol catalyzed by sulfuric acid. To synthesize derivatives **13** and **16**, compounds **12** and **15** were acetylated with acetic anhydride catalyzed by phosphoric acid to give the *O*-acetyl derivatives (Scheme 2). To synthesize compounds **18** and **19** (cardanol series), **9** was converted to the acetoxy (**18**) and methoxy (**19**) derivatives in similar procedures applied in the synthesis of compounds **4** and **17**. To approximate the structural characteristics among the derivatives of anacardic acid, isoanacardic acid, and cardanol, **9** was transformed into α-phenoxyalkyl esters by reaction of **9** with ethyl bromoacetate in acetone at room temperature or ethyl α-bromoisobutyrate in the presence of KI in acetonitrile at 82 °C to give the respective compounds **20** and **21**. Finally, the ethyl esters **20** and **21** were hydrolyzed with LiOH in THF/H_2O in the presence of the phase transfer catalyst Aliquat 336, at room temperature for **20** and at 82 °C for **21**, to provide the α-phenoxyalkyl acids **22** and **23** (Scheme 2).

After preliminary screening of the saturated cardanol derivatives showed selective activation of PPARs (shown below), we synthesized a series of monounsaturated cardanol derivatives (**24**−**27**) to directly compare the impact of the unsaturation in the C15 tail (Scheme 3) to the corresponding saturated derivatives (**20**−**23**).

Biological Evaluation of CNSL Derivatives as PPAR Activators. To examine whether the CNSL derivatives could activate human PPARα, PPARγ, and PPARδ, a luciferase reporter gene assay was performed testing a single concentration of 50 μM in HEK293 cells. The following endogenous fatty acids were also tested: C10:0 (decanoic acid, DA), C14:0 (myristic acid, MA), C18:0 (stearic acid, SA), and C18:1n9 (oleic acid, OA). As shown in Figure 4, this screen identified pan-agonists of all three human PPAR isoforms (**4**, **20**, **22**, **23**, **24**, **25**, **26**, and **27**) and dual agonists for PPARα and PPARγ (C10:0, **3**, **14**, and **21**). Surprisingly, C14:0 and C18:1n9 were only active against PPARα and PPARδ, while C18:0, **5**, and **12** showed significant luciferase activation for PPARα only (Figure 4A−C).

We next determined the relative potency and efficacy of the active CNSL derivatives by performing a full dose−response curve for the three human PPAR isoforms. The activity profiles and half-maximal effective concentration (EC_{50}'s) of fatty acids and our compounds were compared to positive controls that are synthetic agonists with high specificity, full agonist activity, and high potency for their respective PPAR receptor in the luciferase assays. These positive controls were GW7647

https://doi.org/10.1021/acs.jmedchem.1c01542
J. Med. Chem. 2022, 65, 1961−1978

Scheme 2. Synthesis of Isoanacardic Acid and Cardanol Derivatives 9−23[a]

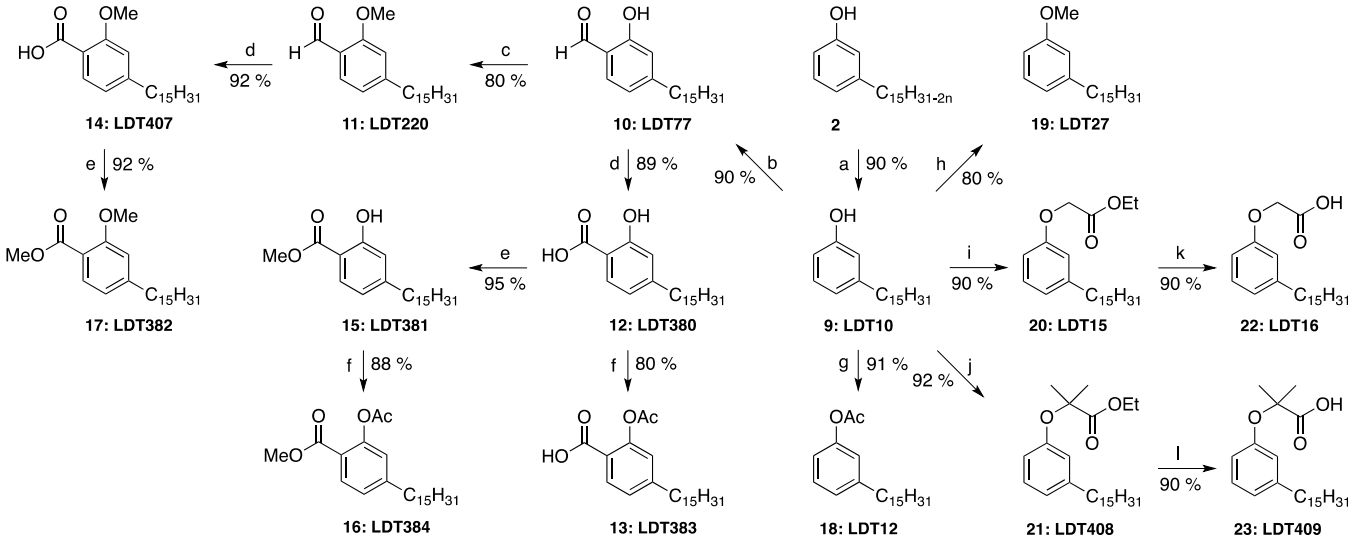

[a]Reagents and conditions: (a) H_2, Pd/C 10%, EtOH, r.t., 4 h; (b) CH_2O, $MgBr_2$, tetrahydrofuran (THF), reflux, 24; (c) MeI, K_2CO_3, Me_2CO, 120°C, 20 h; (d) $NaClO_2$ 1 M, NaH_2PO_4 1 M, DMSO, CH_2Cl_2, r.t., 16 h; (e) MeOH, H_2SO_4, 50 °C, 16 h; (f) AC_2O, H_3PO_4, MW (270 W), 10 min; (g) AC_2O, H_3PO_4, MW (400 W), 3 min; (h) MeI, K_2CO_3, Me_2CO, 65 °C, 24 h; (i) $BrCH_2CO_2Et$, K_2CO_3, Me_2CO, r.t., 24 h; (j) $BrC(CH_3)_2CO_2Et$, KI, K_2CO_3, MeCN, 82 °C, 24 h; (k) LiOH, Aliquat, THF/H_2O, r.t. 4 h; (l) LiOH, Aliquat, THF/H_2O, 65 °C, 4 h.

Scheme 3. Synthesis of Compounds 24−27 from Monounsaturated Cardanol (2A)[a]

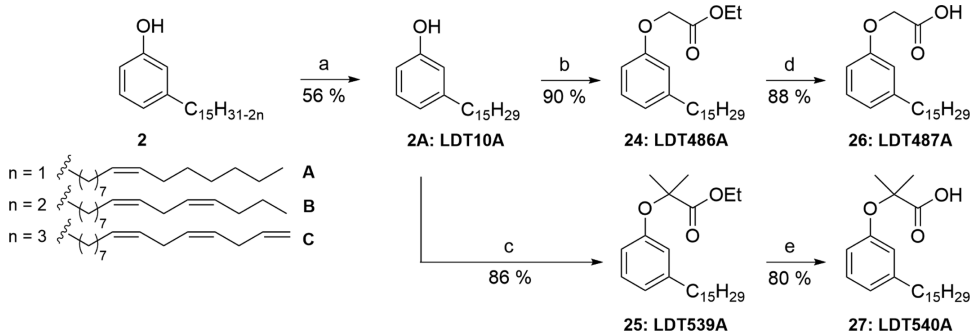

[a]Reagents and conditions: (a) $SiO_2/AgNO_3$ column, hexanes, (b) $BrCH_2CO_2Et$, K_2CO_3, Me_2CO, r.t., 24 h; (c) $BrC(CH_3)_2CO_2Et$, KI, K_2CO_3, MeCN, 82 °C, 24 h; (d) LiOH, Aliquat, THF/H_2O, r.t. 4 h; (e) LiOH, Aliquat, THF/H_2O, 65 °C, 4 h.

(PPARα agonist), rosiglitazone (Rosi, PPARγ agonist), and GW0742 (PPARδ agonist), respectively. Individual E_{max} values were calculated relative to positive controls (set to 100%) and are reported in Figure S1 and summarized in Table 1. For some compounds, solubility was limiting and saturation of the activity was not achieved. Against PPARα, C10:0, C14:0, and C18:0 displayed partial agonist activity compared to GW7647 (Figure S1A). Similarly, **3**, **5**, **12**, **14**, and **20**−**25** partially induced PPARα activity relative to GW7647 (Figure S1A). In contrast, C18:1n9, **4**, **26** and **27** acted as full agonists of PPARα, with equal or greater RLU induction compared to GW7647 (Figure S1A). The EC_{50} values of the CNSL derivatives ranged from 0.5 to 67 μM for PPARα (Table 1). Thus, many were more potent than the endogenous fatty acid ligands which activated PPARα between 13 and 40 μM. Against PPARγ, the CNSL derivatives **14**, **20**, **21**, and **23** displayed partial agonist activity compared to Rosi (Figure S1B). Surprisingly, **3**, **4**, **22**, and **27** exhibited similar or higher maximal activity relative to Rosi, though they were of lower potency, activating PPARγ at micromolar concentrations from 0.9 to 50 μM (Table 1). Interestingly, C10:0 was the only fatty acid tested that showed PPARγ activity (EC_{50} 54 μM, Table 1). No E_{max} could be determined for **24**−**26** because they did not reach saturation against PPARγ. Activation of PPARδ was additionally explored with EC_{50} values for the active compounds (Figure S1C). We found that C14:0, C18:1n9, **3**, **4**, and **22**−**27** partially induced transcriptional activation of human PPARδ compared to GW0742, a full PPARδ agonist with EC_{50} of 3.5 nM (Figure S1C). PPARδ was weakly induced by fatty acids and the CNSL derivatives at micromolar concentrations, ranging from 10 to 100 μM (Table 1). Taken together, a subset of CNSL derivatives were successfully identified as a single, dual, and/or pan-PPAR agonists with partial or full agonistic activities for human PPAR isoforms. These data suggest that these CNSL derivatives represent a new chemical class of PPAR agonists that structurally mimic the endogenous fatty acid ligands of PPARs but generally with higher potency.

CNSL Derivatives Selectively Target PPARα-Responsive Genes for the Regulation of Lipid Metabolism in Primary Hepatocytes. To examine the ability of CNSL derivatives to activate PPARα target genes, mouse primary

https://doi.org/10.1021/acs.jmedchem.1c01542
J. Med. Chem. 2022, 65, 1961−1978

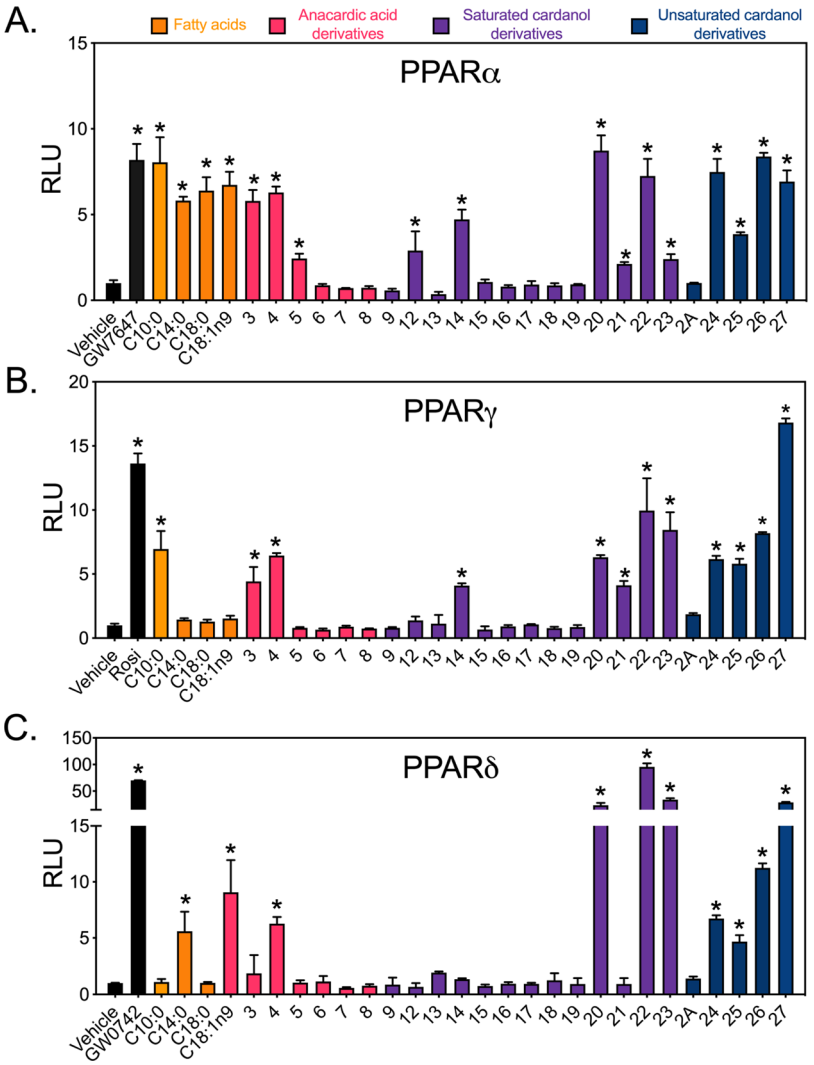

Figure 4. *In vitro* screening of CNSL derivatives for PPARα, PPARγ, and PPARδ activity reveals a subset of selective pan-activators. HEK293 cells were transiently co-transfected with GAL4-hPPARα (A), GAL4-hPPARγ (B), or GAL4-hPPARδ (C) together with UAS-luciferase reporter and treated with positive controls (10 nM GW7647, 100 nM Rosi, and 10 nM GW0742) or 50 μM of indicated compounds for 16 h. Data represent mean ± standard deviation (SD) (N = 3). RLU, relative luciferase units = luciferase light units/β-galactosidase × time. Vehicle (DMSO) response was set to 1. C10:0, decanoic acid; C14:0, myristic acid; C18:0, stearic acid; C18:1n9, oleic acid. *P < 0.05 relative to corresponding vehicle, using one-way analysis of variance (ANOVA) with Holm−Šidák correction.

hepatocytes were treated with 50 μM of the CNSL derivatives for 16 h. Consistent with their ability to activate PPARα, the PPARα agonists, WY14643 (WY) and GW7647 (GW), significantly induced the mRNA expression of genes involved fatty acid uptake such as fatty acid binding protein 1 (*Fabp*1) and *Cd*36 (cluster of differentiation 36) (Figure 5A,B). Notably, dual PPARα/γ agonist, muraglitazar (Mura), also strongly upregulated the expression of *Fabp*1 and *Cd*36, whereas Rosi, the PPARγ agonist, did not. *Fabp*1 and *Cd*36 were significantly increased by **24** and **25**. In contrast, **22** only induced gene expression of *Fabp*1 while **23** and **26** significantly upregulated *Cd*36 (Figure 5A,B). In addition, WY, GW, and Mura significantly increased the fatty acid oxidation genes fibroblast growth factor 21 (*Fgf*21) and pyruvate dehydrogenase 4 (*Pdk*4), whereas induction by Rosi did not reach statistical significance (Figure 5C,D). PPARα-responsive genes *Fgf*21 and *Pdk*4 were robustly increased in primary hepatocytes by **5**, **12**, **22**, **23**, and **27** compared to vehicle control (Figure 5C,D). Intriguingly, **3**, **4**, and **24** increased the mRNA expression of *Pdk*4 but not *Fgf*21 (Figure 5C,D). Additionally, **12** upregulated only the expression of *Fgf*21 and **14** failed to upregulate any of the target genes despite having an EC_{50} for PPARα below that of **5** (17 *vs* 32 μM, respectively). These results suggest that depending on their structure, the CNSL derivatives can promote fatty acid uptake and oxidation in the liver by differential targeting of PPARα binding sites, leading to decreased circulating lipids and improved lipid metabolism.

CNSL Derivatives Differentially Activate PPARγ-Target Genes in the Process of 3T3-L1 Adipocyte Differentiation. PPARγ is considered a master regulator for the differentiation of pre-adipocytes into mature fat cells.[39] Indeed, weight gain is a major side effect of the TZD class of insulin-sensitizing drugs.[40,41] Insulin sensitization, however, requires the activation of PPARγ in adipose to promote the expression of adiponectin (encoded by *Adipoq*), an adipokine that signals *via* the liver and muscle to regulate glucose homeostasis.[42,43] To gain an understanding of whether the

https://doi.org/10.1021/acs.jmedchem.1c01542
J. Med. Chem. 2022, 65, 1961−1978

Table 1. Activity of CNSL Derivatives for Human PPARs *In Vitro*[a,b]

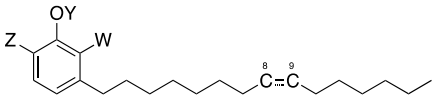

compound		W	Y	Z	C_{8-9}	hPPAR EC_{50} (μM) E_{max} α	γ	δ
anacardic acid derivatives	**3**	CO_2H	H	H	CH_2	3.5[c]	17[d]	68[b]
	4	CO_2H	Ac	H	CH_2	2.4[d]	12[d]	>50[e]
	5	CO_2H	Me	H	CH_2	32[c]	–[f]	–
	6	CO_2Me	H	H	CH_2	–	–	–
	7	CO_2Me	Ac	H	CH_2	–	–	–
	8	CO_2Me	Me	H	CH_2	–	–	–
saturated cardanol derivatives	**9**	H	H	H	CH_2	–	–	–
	12	H	H	CO_2H	CH_2	8.9[c]	–	–
	13	H	Ac	CO_2H	CH_2	–	–	–
	14	H	Me	CO_2H	CH_2	17[c]	8.1[c]	–
	15	H	H	CO_2Me	CH_2	–	–	–
	16	H	Ac	CO_2Me	CH_2	–	–	–
	17	H	Me	CO_2Me	CH_2	–	–	–
	18	H	Ac	H	CH_2	–	–	–
	19	H	Me	H	CH_2	–	–	–
	20	H	CH_2CO_2Et	H	CH_2	3.5[c]	29[c]	>100[e]
	21	H	CMe_2CO_2Et	H	CH_2	8.9[b]	3.9[c]	–
	22[g]	H	CH_2CO_2H	H	CH_2	1.1[c]	3.7[d]	10[c]
	23	H	CMe_2CO_2H	H	CH_2	0.5[c]	0.9[c]	33[c]
unsaturated cardanol derivatives	**2A**	H	H	H	CH=	–	–	–
	24	H	CH_2CO_2Et	H	CH=	4.4[c]	>50[e]	7.1[b]
	25	H	CMe_2CO_2Et	H	CH=	67[c]	>50[e]	>100[e]
	26	H	CH_2CO_2H	H	CH=	21[d]	>50[e]	70[c]
	27	H	CMe_2CO_2H	H	CH=	0.7[d]	1.8[d]	21[c]
fatty acids	C10:0 (DA)					31[c]	54[d]	–
	C14:0 (MA)					13[c]	–	51[b]
	C18:0 (SA)					40[c]	–	–
	C18:1 (OA)					36[d]	–	47[b]
controls	GW7647					0.0065	–	–
	rosiglitazone					–	0.049	–
	GW0742					–	–	0.0035

[a]EC_{50} values were obtained using reporter gene assays. [b]E_{max} 5−29% of the corresponding positive control. [c]E_{max} 30−89% of the corresponding positive control. [d]$E_{max} \geq 90\%$ of the corresponding positive control. [e]Did not reach saturation at the highest concentration tested. [f]–: Not active. [g]Cellular toxicity.

CNSL derivatives would impact adipocyte differentiation and insulin sensitization, 3T3-L1 cells were differentiated in the presence of 25 μM of CNSL derivatives or 10 μM Rosi for 11 days. As expected, Rosi efficiently promoted the differentiation of 3T3-L1 cells into adipocytes, as indicated by the increase in Oil Red O staining relative to vehicle (Figure 6A, quantified in (B)). Interestingly, **3** and **24**−**26** were as efficient as Rosi at promoting adipocyte differentiation (Figure 6A,B). By contrast, **4**, **14**, **20**, **21**, **23**, and **27** showed lower lipid accumulation in differentiated 3T3-L1 cells compared to Rosi (Figure 6A,B). In addition, Rosi significantly increased the expression of key early adipogenic genes, including *PPARγ* itself and CCAAT/enhancer binding protein α (*Cebpα*), as well as genes responsible for fatty acid uptake and storage such as adipocyte binding protein 2 (*aP2*), lipoprotein lipase (*Lpl*), and *Cd36* (Figure 6C−G). Additionally, Rosi significantly upregulated the mRNA expression of the beneficial adipokine *Adipoq* and insulin-stimulated glucose uptake transporter glucose transporter type 4 (*Glut4*) (Figure 6H,I). We noted that CNSL derivatives were less effective at inducing genes that were involved in fatty acid update and adipogenesis compared to Rosi (Figure 6C−G), yet some CNSL derivatives still strongly induced the expression of *Adipoq* and *Glut4*, including **23** and **27**, which had levels at or above those induced by Rosi (Figure 6H−I). These data indicate that CNSL derivatives may be beneficial for the treatment of insulin resistance without the severe consequence on body weight. No data could be obtained for **22** in 3T3-L1 cells as it was found to be toxic over the time period required for differentiation. It is unclear why **22** is selectively toxic in 3T3-L1 and HEK293 cells (Table 1), but not primary hepatocytes (Figure 5). An 3-(4,5-dimethylthiazol-2-yl)-2,5-diphenyltetrazolium bromide (MTT) assay performed in HEK293 cells dosing CNSL derivatives at 25 μM found that only **22** showed significant toxicity (data not shown). In summary, **20**, **21**, **23**, and **27** show selective PPARγ target gene activation in 3T3-L1 cells that could potentially separate their effects on adipocyte differentiation from its favorable glucose-lowering effects.

In Vivo Screening of the CNSL Derivatives in Zebrafish Embryos Harboring Transgenic Human

https://doi.org/10.1021/acs.jmedchem.1c01542
J. Med. Chem. 2022, 65, 1961−1978

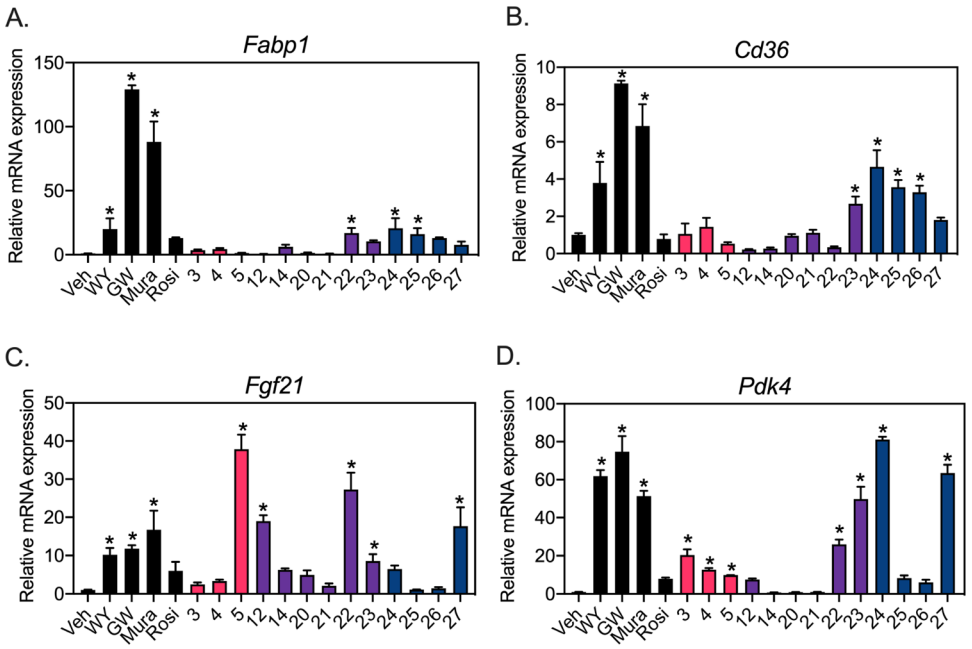

Figure 5. CNSL derivatives activate PPARα target genes in primary hepatocytes in a gene-selective manner. Primary hepatocytes were isolated from wild-type (WT) mice and incubated with vehicle (Veh, DMSO), 50 μM CNSL derivatives or 10 μM of positive controls: WY14643 (WY, PPARα agonist), GW7647 (GW, PPARα agonist), muraglitazar (Mura, PPARα/γ agonist), rosiglitazone (Rosi, PPARγ agonist) for 16 h. Expression of fatty acid uptake genes *Fabp*1 (A) and *Cd*36 (B), and fatty acid oxidation genes, *Fgf*21 (C) and *Pdk*4 (D) were analyzed by quantitative polymerase chain reaction (QPCR). Veh mRNA expression was set to 1. Data represent mean ± SD (N = 3). *P < 0.05 vs Veh using one-way ANOVA with Holm−Šidák correction.

PPARs. To assess the *in vivo* activity and tissue distribution of the CNSL derivatives, we used the ligand trap zebrafish screening system. In this model, fusion proteins of the GAL4 DNA binding domain and the ligand-binding domain (LBD) of human PPARs are expressed under the control of a heat shock promoter.[44] A green fluorescent protein (GFP) reporter responsive to GAL4 binding is included in the transgene so that after exposure to heat shock, the 2-day post-fertilization embryos express GFP in tissues where their endogenous respective PPAR ligand is present (Figure 7, vehicle). In the presence of exogenously added WY14643, full agonist for PPARα, GFP expression in embryos expands from its relatively restricted pattern to include strong expression in the CNS, epidermis, heart, retina, and muscle. Rosiglitazone treatment strongly increased PPARγ activity in the tail bud, CNS and heart. In contrast, GW0742 increased PPARδ activity in CNS and muscle. All CNSL derivatives were dosed at each receptor's EC_{50}, unless otherwise indicated, to allow us to compare the signal intensity and tissue distribution between compounds and account for their varied affinities. **4** and **23** strongly activated PPARα in the brain, yolk sac, heart, and muscle. In contrast, **21** and **27** demonstrated restricted activation of PPARα, predominantly in brain. Compared to activation by Rosi, CNSL derivatives were mostly active in tail bud (**4**, **23**, **27**), forebrain (**23**, **27**) and hindbrain (**23**, **27**) in the PPARγ fish line. In the PPARδ zebrafish line, there was substantial basal activity and none of the tested CNSL derivatives increased GFP signal beyond vehicle. Interestingly, **20** did not activate any of the PPARs suggesting there are *in vivo* barriers that preclude it from accessing the PPARs. These data support the value of an *in vivo* screening system since this differential response could not be predicted based on the EC_{50} values or gene expression performed by *in vitro* screening alone. Overall, these data suggest that selected CNSL derivatives (**4**, **21**, **23**, **27**) reveal tissue-specific activation of PPARα and/or PPARγ in an *in vivo* zebrafish embryo model.

Selected CNSL Derivatives Bind and Stabilize the hPPAR-LBDs. To determine whether the CNSL derivatives bound directly to PPARs, we performed a thermal shift assay with purified hPPARα-, hPPARγ-, and hPPARδ-ligand-binding domains (LBDs). Direct binding of a ligand to purified LBD protein should lead to stabilization against thermal denaturation. We found that **4**, **23**, and **27** induced large thermal shifts for the PPARα, PPARγ, and PPARδ LBDs with midpoint melting temperatures (T_m) that were +4 to +17 °C higher than the T_m of DMSO control groups (Figure 8A−C). These shifts were similar or greater than what we observed with each receptor's positive control: GW7647, rosiglitazone, and CAY10512 had ΔT_m values of +5.2, +5, and +7.7 °C, respectively (Figure 8A−C). In contrast, a negative thermal shift was observed when **20** was incubated with the LBDs of PPARα and PPARγ (Figure 8A,B), whereas, **21** had no effect on the T_m values for all three PPARs. These data suggest **20** and **21** do not directly interact with the ligand-binding pockets. Given that both **20** and **21** are ethyl esters, they would require de-esterification prior to binding the PPAR LBDs, a process that could occur only with intact cells. These results suggest that **4**, **23**, and **27** directly interact and stabilize the ligand-binding domains of PPARα, PPARγ, and PPARδ.

***In Silico* Docking of 23 to PPARα, PPARγ, and PPARδ Uncovers Key H-Bonding and Unique Hydrophobic $\pi-\pi$ Interactions Not Present with Endogenous Fatty Acids.** Based on our extensive docking calculations of compounds **3**, **4**, and **20**−**23** with Glide SP and XP scoring functions, and Induced-Fit Docking (IFD) protocol, which produced similar results, we expected the carboxylic group of CNSL to bind within the ligand-binding domain of PPAR receptors (Figure S2A−C, with compound **23** bound), forming

https://doi.org/10.1021/acs.jmedchem.1c01542
J. Med. Chem. 2022, 65, 1961−1978

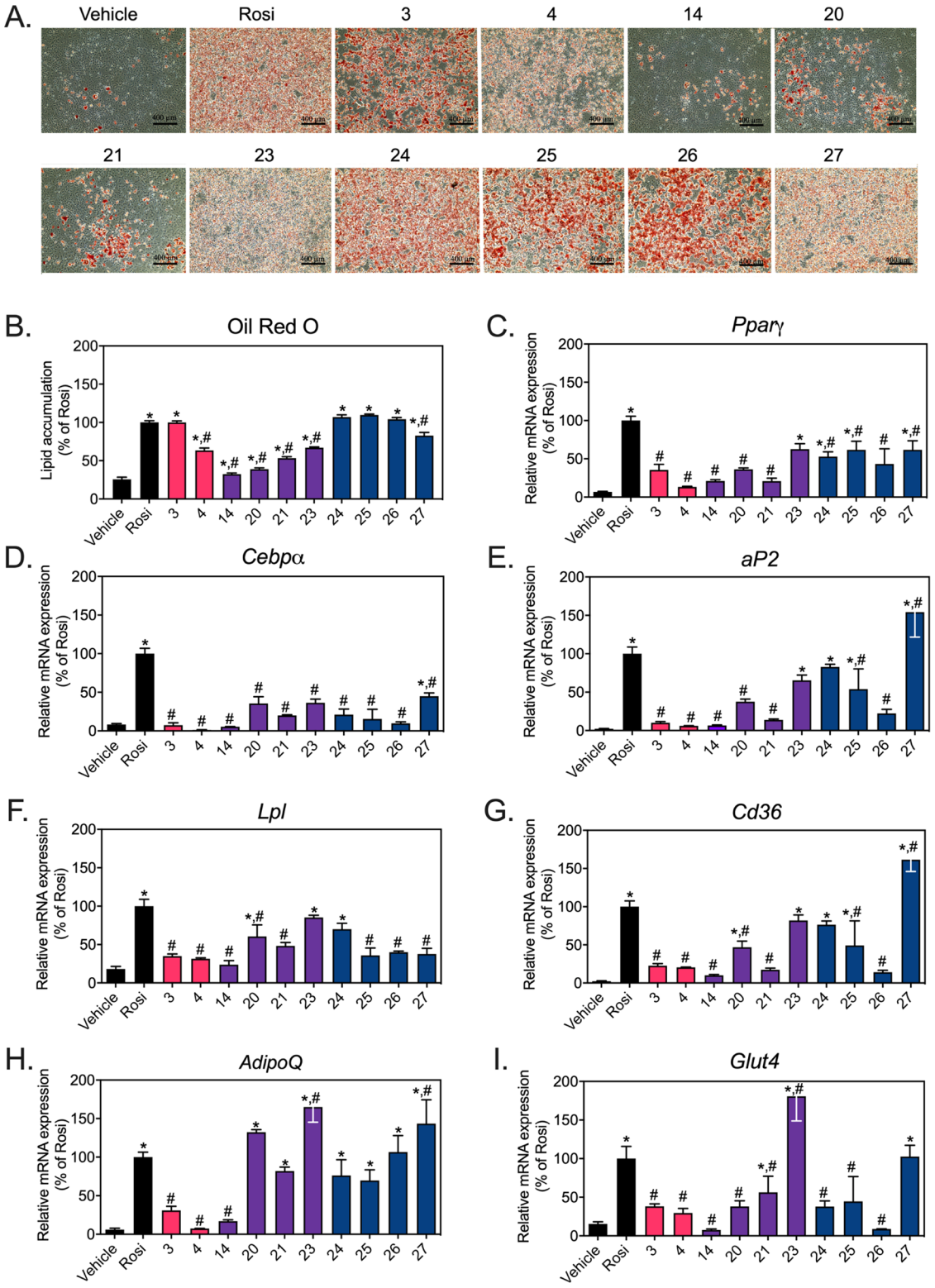

Figure 6. CNSL derivatives differentially regulate the expression of PPARγ target genes and adipocyte differentiation in 3T3-L1 cells. 3T3-L1 fibroblasts were differentiated for 11 days in the presence of vehicle (DMSO), 25 μM of indicated CNSL derivatives or 10 μM rosiglitazone (Rosi). Cells were harvested for Oil Red O staining and mRNA on day 11. (A) Cells were imaged under 10× magnification (n = 2/per group). (B) Lipid accumulation was quantitated by spectrophotometric analysis of extracted Oil Red O. mRNA expression was analyzed by QPCR for two key regulators of adipogenesis, (C) *Pparγ* and (D) *Cebpα*; fatty acid uptake genes (E) *aP2* (*Fabp4*), (F) *Lpl*, and (G) *Cd36*; adipose-specific adipokine gene (H) *AdipoQ* and glucose uptake gene (I) *Glut4*. Vehicle mRNA expression was set to 1 and Rosi value was set to 100%. Data represent mean ± SD (N = 3). *P < 0.05 vs vehicle and $^{\#}P$ < 0.05 vs Rosi; using one-way ANOVA with Holm−Šidák correction.

four strong and essential hydrogen (H)-bonds with the surrounding polar residues of PPARα (S280, Y314, H440, and Y464[45]) and PPARγ (S289, H323, H449, and Y473[46−48]) (Figure S2D,E). This is not the case with PPARδ, where CNSL

https://doi.org/10.1021/acs.jmedchem.1c01542
J. Med. Chem. 2022, 65, 1961−1978

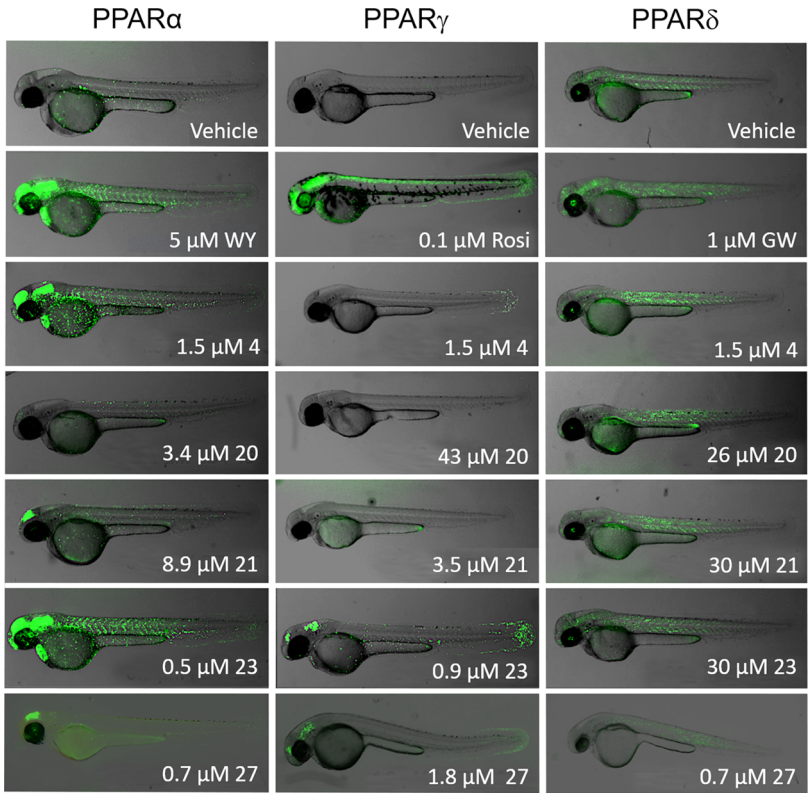

Figure 7. *In vivo* testing of CNSL derivatives using transgenic zebrafish that express human PPARα, PPARγ, or PPARδ reveal tissue-specific activation. Activation of human PPAR in the zebrafish embryo results in GFP expression. Basal activity of PPARα, PPARγ, and PPARδ is observed with vehicle (DMSO) treatment and is strongly increased in the presence of the full agonist for each receptor. Positive controls are WY (WY14643) for PPARα, Rosi (rosiglitazone) for PPARγ, and GW (GW0742) for PPARδ, respectively. Compounds were screened at their respective EC_{50}'s determined from their dose−response curves in HEK293 cells with a few exceptions: **4** was screened at 1.5 μM for all receptors because of toxicity at higher concentrations; for PPARδ, **20** and **27** were screened below their EC_{50}'s due to toxicity at higher concentrations. Each image depicts a representative embryo. Note that embryos incubated with **27** were imaged using a different microscope.

form only one strong H-bond with Y437 and two weaker H-bonds with H413 and H287,[49] and no H-bonding interaction with T253 when we used 3U9Q structure of PPARδ for the docking calculation. These results agree with the thermal stabilization assay, indicating the structural key for the highest PPARα/γ activity/selectivity is the carboxylic group engagement. As a result, we hypothesized that the activity of the CNSL derivatives was highly dependent on the ability to form these four strong H-bonds with their carboxylic functional groups. The long 15 carbon aliphatic chains of the CNSL derivatives fold very well within the hydrophobic pockets. We found unique $\pi-\pi$ interactions between the phenyl group of the CNSL derivatives with the histidine side chains located in the hydrophobic pocket of each receptor (H440 in PPARα, H449 in PPARγ and H413 in PPARδ). In addition, the *gem*-dimethyl group of **23** fits well in the hydrophobic pocket, formed by Q277, V444, and L456 in PPARα; Q286, L453, and L465 in PPARγ; and Q250, M417, and L429 in PPARδ (not shown). In contrast, with the anacardic acid derivative **4**, the phenyl moiety gains similar $\pi-\pi$ stacking interactions with the histidine side chains of the PPAR isoforms. These $\pi-\pi$ stabilizing stacking interactions are not possible with the fatty acid ligands that lack the phenyl ring.

It is known that proteins are very dynamic and X-ray crystal structures that represent a static snapshot of a protein, are packed in a crystal, and are frozen at a liquid nitrogen temperature. To investigate the stability of the key H-bonds formed by the polar warhead of **23** we conducted 10 ns molecular dynamics simulations using Desmond (D. E. Shaw Research) using NPT ensembles at 310 K constant temperature and 1 atm constant pressure using the OPLS3 force field. Average distances for the key interactions (H-bond, $\pi-\pi$, and cation$-\pi$ interactions) as well as the percentage of time they were observed during the simulation were different for the three PPAR isoforms (Figure S3). We observed that all four key H-bonds were observed during 98−99% of the simulation time in PPARα. In the case of PPARγ, only three H-bonds remained very stable, while the H323 H-bond was only formed 88% of the time. The situation was even worse in the case of PPARδ. In this isoform, only the Y437 H-bond was very stable, all other H-bonds were formed and remained stable only 69, 79, and 80% of the time for H287, H413, and T253, respectively (Figure S3). It is worth noting that during the docking calculation compound **23** did not form a H-bond with T253 (Figure S2F). This is due to the fact that the conformation of the T253 side chain in the 3U9Q structure of PPARδ precludes the formation of this H-bond. During the 10 ns molecular dynamics run, the side chain of T253 was able to flip and form the H-bond with one of the carboxylate oxygens of **23** 80% of the time. These observations are consistent with the relative potency of **23** against the α-, γ- and δ-PPAR isoforms of 0.5, 0.9 and 33 μM, respectively. Also, analysis of the dynamic structure of the proteins using fully solvated, long molecular dynamics simulations shed more light on the nature and stability of protein−ligand interactions.

https://doi.org/10.1021/acs.jmedchem.1c01542
J. Med. Chem. 2022, 65, 1961−1978

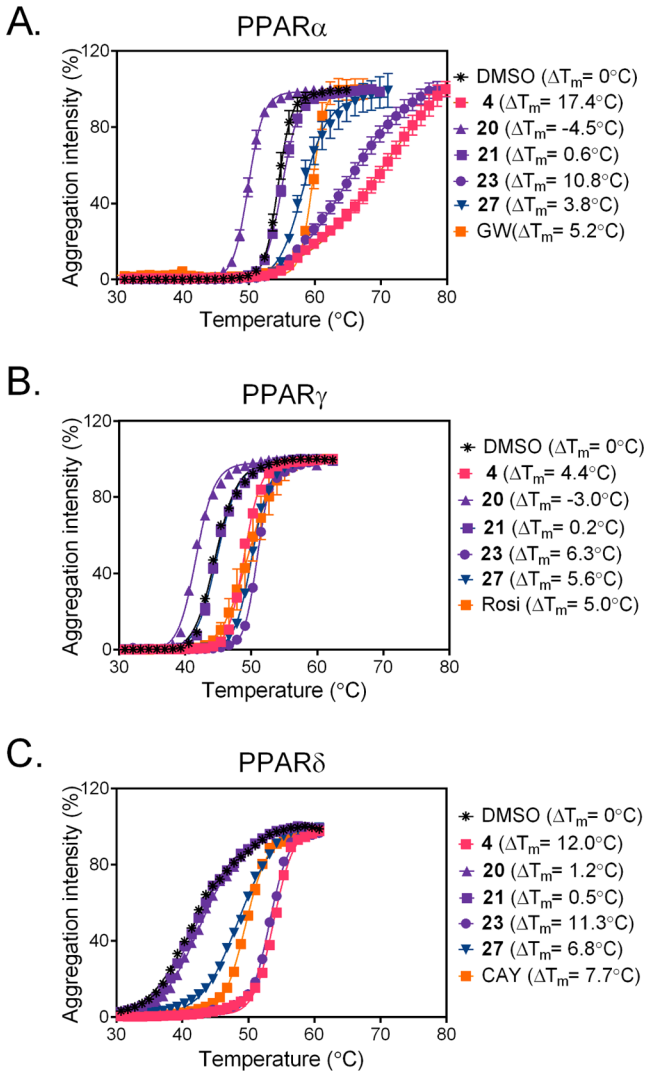

Figure 8. Thermostabilization of hPPARα-LBD, hPPARγ-LBD, and hPPARδ-LBD by carboxylic acid-containing CNSL derivatives. Thermal shift assays of hPPARα-LBD (A) interacting with 25 μM GW7647 or 25 μM CNSL derivatives. Stabilization of the hPPARγ-LBD (B) and the hPPARδ-LBD (C) by 50 μM Rosi (rosiglitazone), 50 μM CAY (CAY10592), or 50 μM CNSL derivatives, respectively. The temperature−response curves were analyzed using the four-parameter dose−response curve function in GraphPad Prism 8 and T_m values were determined. ΔT_m values were calculated for each compound relative to DMSO and are listed in the legend. Data points represent mean ± standard error of the mean (SEM) (N = 3).

***In Vitro* Metabolic Stability of the CNSL Derivatives and Pharmacokinetic (PK) Profile of 23 in C57Bl/6 Mice.** We investigated the metabolic stability of the most active CNSL derivatives *in vitro* using mouse liver microsomes by measuring the rate of disappearance of the parent compound over time (0, 120 min) (Table 2). The cardanol derivatives **20**, **21**, **23**, and **27** all displayed high stability ($t_{1/2}$ > 2 h), whereas the anacardic acid derivative **4** had a short half-life of only 2 min (Table 2).

Next, we performed a pharmacokinetic study of **23** in mice. Compound **23** (LDT409) was selected for further study because of its promising *in vitro* profile that identified it as a relatively potent (EC_{50} < 1 μM), stable ($t_{1/2(microsomes)}$ > 2 h), dual partial agonist of PPARα and PPARγ and showed selective tissue activation in the *in vivo* zebrafish models. A

Table 2. Mouse Liver Stability of Selected CNSL Derivatives *In Vitro*[a]

compound ID	liver microsomal $t_{1/2}$ (min)	% remaining at 120 min
4	2.0 ± 1.4[b]	0
20	66 ± 14	28 ± 8
21	335 ± 20	78 ± 5
23	360 ± 40	79 ± 3
27	835 ± 140	90 ± 5

[a]Results are expressed as mean ± SD (N = 3). [b]To assess the rate of disappearance of **4**, time points of 2.5 and 5 min were used.

single dose of **23** was administered to C57BL/6 male mice either intraperitoneally (40 mg/kg) or orally (100 mg/kg) and plasma was collected for analyte analysis by liquid chromatography/tandem mass spectrometry (LC/MS/MS) (Figure 9). The resulting pharmacokinetic parameters are presented in Table 3. The maximum concentration (C_{max}) and half-life were 102 ± 12 mg/L and 4.0 h, respectively, after intraperitoneal (IP) administration of 40 mg/kg. After oral administration, the C_{max} was 76 ± 5 mg/L (100 mg/kg dose), indicating a good relative bioavailability (F_{rel}) against the IP dose of 38% (Table 3). The terminal half-life was calculated to be 2.3 h after oral dosing, and **23** was almost completely eliminated within 24 h (Figure 9B). These data support the potential for chronic daily dosing of **23** in mice as they suggest that such dosing regimens would result in plasma concentrations above the respective PPARα/PPARγ EC_{50}'s for at least 16 h.

CONCLUSIONS

Herein, we report the design and synthesis of novel compounds derived from anacardic acid and cardanol, phenolic lipids that are abundant in CNSL, the waste byproduct of the cashew nut industry. Importantly, these derivatives retained structural similarity to fatty acids that are known to endogenously activate PPARs. When tested against a panel of PPAR receptors *in vitro*, several compounds were found to be single-, dual-, or pan-PPAR agonists with partial agonist activity and low micromolar potency. Detailed characterization of adipocyte and hepatocyte responses, and *in vivo* biodistribution studies in zebrafish embryos led to the identification of the lead compound, **23** (LDT409), which is a novel partial pan-PPAR agonist with potent and balanced affinity for PPARα and PPARγ and weak binding affinity to PPARδ. Notably, markers of the beneficial glucose-lowering effects of PPARγ agonists (Rosi) in adipocytes were retained with **23**. Overall, based on the desirable *in vitro* pharmacological activity results and the favorable *in vivo* pharmacokinetic profile, **23** may represent a sustainable resource from which to generate affordable agents to treat dyslipidemia and type 2 diabetes.

EXPERIMENTAL SECTION

General Procedures. Chemicals were purchased from Sigma-Aldrich (Brazil and Canada). Decanoic, myristic, stearic, and oleic acids were purchased from Sigma-Aldrich. Cardanol mixture was donated by Resibras/Cashol (Fortaleza, Brazil). Hydrogenation were performed in a shaker hydrogenation apparatus (Paar Instruments). The acetylation reactions were performed in a household microwave Brastemp BMK38ABHNA model and power 900 W. Chromatographic separations were performed using silica gel columns by flash (silica gel 60, 230−400 and 70−230 mesh, Silicycle) chromatography with the solvent mixtures specified in the corresponding experiment. The progress of the reactions was observed by thin-layer

https://doi.org/10.1021/acs.jmedchem.1c01542
J. Med. Chem. 2022, 65, 1961−1978

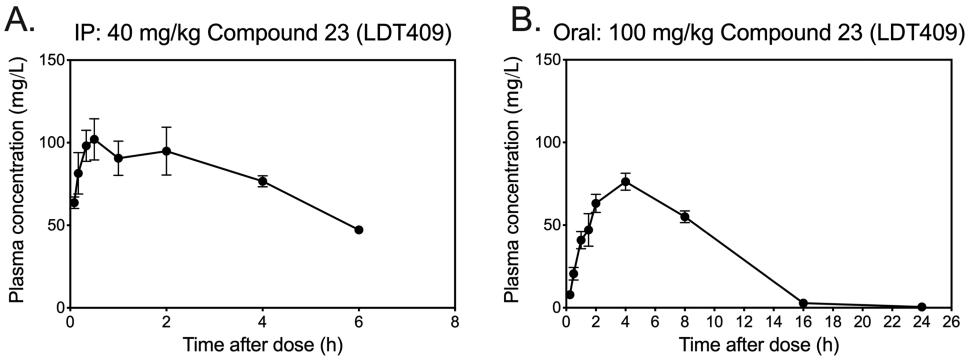

Figure 9. *In vivo* pharmacokinetic profile of **23** (LDT409) in C57BL/6 mice. The plasma concentration of **23** (LDT409) in mice after (A) a single intraperitoneal injection (IP) at 40 mg/kg and (B) oral administration in peanut butter treat at 100 mg/kg. Data represent mean ± SEM ($N = 4$ per time point).

Table 3. Pharmacokinetic Parameters of 23 (LDT409) in Mice after a Single IP and Oral Administration[a]

parameters	units	40 mg/kg (IP dose)	100 mg/kg (oral dose)
C_{max}	mg/L	102 ± 12	76 ± 5
C_{min}	mg/L	47 ± 3	0.5 ± 0.3
$AUC_{0-\infty}$	mg h/L	748	717
k_e	h^{-1}	0.174	0.298
$t_{1/2}$	h	4.0	2.3
t_{max}	h	0.5	4
CL/F	mL/(min kg)	0.89	2.3
F_{rel}	%		38

[a]Results are presented as mean ± SEM. $AUC_{0-\infty}$, area under the concentration−time curve from zero to infinity; C_{max}, maximal concentration; C_{min}, minimum concentration; CL, clearance; F, bioavailability; F_{rel}, relative bioavailability (oral *vs* IP); k_e, elimination rate constant; $t_{1/2}$, half-life; t_{max}, time of maximum concentration observed.

chromatography (TLC) on Silicycle (0.25 mm) precoated silica gel plates (60 F254), then visualized with ultraviolet light (254 nm). Melting points (mp) were determined in open capillaries on a Quimis MQAPF 302 melting point apparatus and are uncorrected. Hydrogen (^{1}H) and carbon (^{13}C) NMR spectra were recorded on a Bruker Avance DRX500 (499.70 MHz for ^{1}H; 125.66 MHz for ^{13}C) or DRX300 (300.13 MHz for ^{1}H; 75.47 MHz for ^{13}C) using $CDCl_3$ or Pyr-d_5 as solvents. Chemical shifts are reported in parts per million (ppm) relative to tetramethylsilane (TMS), and multiplicity are given as singlet (s), broad singlet (br s), doublet (d), double doublet (dd), triplet (t), quartet (q), multiple (m), or broad signal (bs). IR spectra were recorded on a PerkinElmer Spectrum BX. High-resolution mass spectrometry (HRMS) was acquired on a TripleTof 5600+ (Sciex). Analysis was performed by flow injection using a liquid chromatographer (Eksigent UltraLC 100, Sciex) at a 0.3 mL/min flow. Spectra were acquired using a DuoSpray Ion Source (ESI) in the positive mode in a 100−1000 Da mass range using external calibration. From all new compounds, satisfactory high-performance liquid chromatography (HPLC) analyses were obtained, confirming 95% or higher purity. The instrument was a Shimadzu system [degassing unit (DGU-20A$_{5R}$), two semipreparative solvent delivery units (LC-20AR), a photodiode-array detector (PDA, SPD-M20A), an autosampler (SIL-10AF), and a controller communication bus module (CBM-20A)]. The column was a reversed-phase octadecylsilyl column (4.6 μm, 4.6 × 250 mm^2, Shim-pack VP-ODS). The mobile phase was HPLC-grade acetonitrile containing 0.1% (v/v) trifluoroacetic acid (eluent A) at a flow rate of 1 mL/min. Samples were diluted in eluent A at a concentration of 1 mg/mL. Using the autosampler, 80 μL of each sample was injected and the absorbance at the 200−400 range was monitored for 40 min.

Materials. The mixture of distilled cardanols (**2**) was supplied by the company Resibras/Cashol.

*(Z)-(3-Pentadec-8-en-1-yl)phenol (**2A**, LDT10A).* The mixture of cardanols (**2**) (10.0 g) was purified by a chromatographic column containing silica gel doped with 12% silver nitrate and eluted with a mixture of hexanes, providing derivative **2A** as a pale-yellow oil; yield 56% (5.6 g, 18.5 mmol). ^{1}H NMR (500.13 MHz, $CDCl_3$, ppm) δ 7.15 (t, J = 7.7 Hz, 1H); 6.76 (d, J = 7.4 Hz, 1H); 6.67−6.65 (m, 2H); 5.40−5.34 (sl, 2H); 2.56 (t, J = 7.7 Hz; 2H); 2.08−2.03 (m, 4H); 1.61−1.60 (m, 2H); 1.32−1.24 (m, 16H); 0.92−0.89 (t, J = 6.5 Hz, 3H); ^{13}C NMR (125.66 MHz, $CDCl_3$, ppm) δ 155.7, 145.1, 130.1−130.0, 129.5, 121.1, 115.5, 112.7, 36.0, 32.0, 31.4, 29.9−29.2, 27.4, 22.8, 14.3.

*2-Hydroxy-6-pentadecylbenzoic Acid (**3**, LDT11).* To a solution of 5.0 g of the mixture **1** (~14.4 mmol) in ethanol (50 mL) was added 0.2 g of 10% palladium on carbon (2 mol %), and the mixture was shaken in a Parr apparatus, under hydrogen atmosphere (60 psi) for 6 h. Then, the reaction mixture was filtered in a sintered funnel. The solvent was evaporated under reduced pressure, and the residue was recrystallized from hexane to afford **3** as a white solid. Yield 70% (3.5 g, 10.1 mmol). HPLC purity: 97%. mp 81−84 °C. IR (KBr, cm^{-1}): 3326, 2954, 2920, 2850, 1610, 1542, 1498, 1466, 1466, 1287, 1086. ^{1}H NMR (300.13 MHz, $CDCl_3$, ppm): 10.73 (s, 1H), 7.37 (dd, J = 8.0, 7.4 Hz, 1H), 6.89 (d, J = 8.0 Hz, 1H), 6.79 (d, J = 7.4 Hz, 1H), 3.00 (t, J = 7.7 Hz, 2H), 1.62−1.57 (m, 2H), 1.26 (br, 24H), 0.89 (t, J = 6.5 Hz, 3H). ^{13}C NMR (75.47 MHz, $CDCl_3$, ppm) δ 176.5, 163.8, 148.1, 135.6, 123.0, 116.1, 110.6, 36.7, 32.2, 32.1, 30.0−29.6, 22.9, 14.3; HRMS (ESI+): m/z [(M + H)$^+$] calcd for $C_{22}H_{36}O_3$: 349.2698, found 349.2737.

*2-Acetoxy-6-pentadecylbenzoic Acid (**4**, LDT13).* Compound **3** (3.0 g, 8.6 mmol), acetic anhydride (3.3 mL), and phosphoric acid (six drops) were placed in an Erlenmeyer inside an unmodified household microwave oven and irradiated for 3 min (3 × 1′) at a power of 400 W. After the completion of the reaction, the mixture was extracted with ethyl acetate (3 × 20 mL), and organic phases together were washed with a solution of 5% sodium bicarbonate (20 mL), brine (20 mL), and dried over anhydrous sodium sulfate. The residue was concentrated under reduced pressure and purified by chromatography (silica gel, using a gradient of a mixture hexane/ethyl acetate) to afford **4** as a white solid. Yield 76% (2.6 g, 6.6 mmol). HPLC purity: 96%. mp 65−69 °C. IR (KBr, cm^{-1}): 2922, 2850, 1763, 1701, 1465, 1369, 1221. ^{1}H NMR (300.13 MHz, $CDCl_3$, ppm) δ 7.41 (dd, J = 8.0, 7.5 Hz, 1H), 7.17 (d, J = 7.5 Hz, 1H), 7.01 (d, J = 8.0 Hz, 1H), 2.81 (t, J = 7.8 Hz, 2H), 2.30 (s, 3H), 1.67−1.60 (m, 2H), 1.31−1.26 (m, 24H), 0.89 (t, J = 6.6 Hz, 3H). ^{13}C NMR (75.47 MHz, $CDCl_3$, ppm) δ 172.2, 169.6, 148.8, 143.8, 131.5, 127.7, 125.0, 120.8, 34.1, 32.1, 31.6, 29.9−29.5, 22.9, 21.0, 14.3. HRMS (ESI+): m/z [(M + Na)$^+$] calcd for $C_{24}H_{38}O_4$ 413.2662, found 413.2654.

*Methyl 2-Methoxy-6-pentadecylbenzoate (**8**, LDT28).* Compound **3** (2.0 g, 5.7 mmol) and potassium carbonate (2.4 g, 17.2 mmol) were dissolved in acetone (30 mL). The mixture was stirred

https://doi.org/10.1021/acs.jmedchem.1c01542
J. Med. Chem. 2022, 65, 1961−1978

for 20 min, and then 1.49 mL of methyl iodide (22.9 mmol) was added. The reaction was stirred at 120 °C, for 18 h. Then, the mixture was concentrated under reduced pressure and extracted with ethyl ether (30 mL). The organic phase was washed with a 10% hydrochloric solution (2 × 15 mL), brine (20 mL), and dried with anhydrous sodium sulfate. The solvent was evaporated under reduced pressure, and the product was purified by chromatography (silica gel, using a gradient of a mixture hexane/ethyl acetate) to afford **8** as a white solid. Yield 97% (2.1 g, 5.6 mmol). HPLC purity: 96%. mp 32−33 °C. IR (film, cm^{-1}): 2918, 2850, 1733, 1586, 1466, 1266. ^1H NMR (300.13 MHz, $CDCl_3$, ppm) δ 7.27 (dd, J = 8.3, 7.6 Hz, 1H), 6.82 (d, J = 7.6 Hz, 1H), 6.76 (d, J = 8.3 Hz, 1H), 3.91 (s, 3H), 3.82 (s, 3H), 2.55 (t, J = 7.8 Hz, 2H), 1.61−1.53 (m, 2H), 1.26 (m, 24H), 0.89 (t, J = 6.3 Hz, 3H). ^{13}C NMR (75.47 MHz, $CDCl_3$, ppm) δ 169.1, 156.4, 141.6, 130.4, 123.7, 121.7, 108.5, 56.0, 52.2, 33.6, 32.1, 31.3, 29.8−29.5, 22.8, 14.2. HRMS (ESI+): m/z [(M + H)$^+$] calcd for $C_{24}H_{40}O_3$: 377.3050, found 377.3049.

*2-Methoxy-6-pentadecylbenzoic Acid (**5**, LDT30).* Compound **8** (4.0 g, 10.6 mmol) was dissolved in DMSO (20 mL), and to the solution was added 1.3 g of potassium *tert*-butoxide (10.6 mmol). The reaction mixture was stirred at room temperature for 2 h and then heated to 40 °C for 16 h. Then, the reaction mixture was cooled in ice water, adjusted to pH 2 with 10% hydrochloric solution, and extracted with ethyl acetate (3 × 15 mL). The organic phase was washed with brine (20 mL), dried with anhydrous sodium sulfate, and concentrated under reduced pressure. The product was purified by chromatography (silica gel, using a gradient of a mixture hexane/ethyl acetate), affording **5** as a white solid. Yield 98% (3.8 g, 10.4 mmol). HPLC purity: 96%. mp 74−77 °C. IR (KBr, cm^{-1}): 3365, 2954, 2920, 2848, 1715, 1585, 1473, 1460, 1437, 1316, 1266. ^1H NMR (300.13 MHz, $CDCl_3$, ppm) δ 7.34−7.27 (dd, J = 8.2, 7.6 Hz, 1H), 6.88 (d, J = 7.6 Hz, 1H), 6.81 (d, J = 8.2 Hz, 1H), 3.89 (s, 3H), 2.73 (t, J = 7.8 Hz, 2H), 1.67−1.60 (m, 2H), 1.33−1.26 (m, 24H), 0.89 (t, J = 6.6 Hz, 3H). ^{13}C NMR (75.13 MHz, $CDCl_3$, ppm) δ 173.0, 156.8, 142.7, 131.0, 122.3, 122.2, 108.8, 56.2, 33.9, 32.1, 31.5, 29.9−29.5, 22.9, 14.3. HRMS (ESI+): m/z [(M + H)$^+$] calcd for $C_{23}H_{38}O_3$: 363.2894, found 363.2900.

*Methyl 2-Hydroxy-6-pentadecylbenzoate (**6**, LDT29).* Compound **3** (1.0 g, 2.9 mmol) was dissolved in methanol (25 mL). To the solution, cooled in an ice/water bath, concentrated H_2SO_4 (1.5 mL) was carefully added, and the reaction was stirred under reflux for 18 h. Then, the reaction was extracted with dichloromethane (3 × 10 mL), washed with brine solution (10 mL), and dried with anhydrous sodium sulfate. The solvent was evaporated under reduced pressure, and the product was purified by chromatography (silica gel, using a gradient of a mixture hexane/ethyl acetate) to afford **6** as a white solid. Yield 86% (0.9 g, 2.4 mmol). HPLC purity: 97%. mp 37−40 °C. IR (KBr, cm^{-1}): 3433, 2917, 2851, 1663, 1451, 1250, 1203. ^1H NMR (500.13 MHz, $CDCl_3$, ppm) δ 11.13 (s, 1H), 7.31−7.27 (dd, J = 8.1, 7.3 Hz, 1H), 6.84 (d, J = 8.1 Hz, 1H), 6.73 (d, J = 7.3 Hz, 1H), 3.96 (s, 3H), 2.89 (t, J = 7.8 Hz, 2H), 1.55−1.51 (m, 2H), 1.32−1.27 (m, 29H), 0.89 (t, J = 6.8 Hz, 3H). ^{13}C NMR (125.66 MHz, $CDCl_3$, ppm) δ 172.1, 162.8, 146.4, 134.3, 122.6, 115.8, 112.0, 52.3, 36.8, 32.3, 32.1, 30.1−29.5, 22.9, 14.3. HRMS (ESI+): m/z [(M + H)$^+$] calcd for $C_{23}H_{38}O_3$: 363.2870, found 363.2890.

*Methyl 2-Acetoxy-6-pentadecylbenzoate (**7**, LDT208).* Compound **6** (0.4 g, 1.2 mmol) was solubilized in dichloromethane (6 mL), followed by the addition of triethylamine (3.0 mmol) and acetyl chloride (0.12 mL). The reaction mixture was stirred at room temperature for 24 h, then washed with distilled water, and extracted with ethyl acetate (3 × 10 mL). The combined organic fractions were washed with 5% sodium bicarbonate solution (3 × 10 mL), 10% hydrochloric acid solution (2 × 10 mL), and brine (10 mL) and dried over anhydrous sodium sulfate. After concentrated under reduced pressure, the product was purified by chromatography (silica gel, using a gradient of a mixture hexane/ethyl acetate), affording **7** as a white solid. Yield 58% (0.3 g, 0.7 mmol). HPLC purity: 99%. mp 30−35 °C. IR (KBr, cm^{-1}): 2916, 2850, 1731, 1473, 1368, 1246. ^1H NMR (300.13 MHz, $CDCl_3$, ppm) δ 7.35 (dd, J = 8.0, 7.6 Hz, 1H), 7.12 (d, J = 7.6 Hz, 1H), 6.97 (d, J = 8.0 Hz, 1H), 3.89 (s, 3H), 2.67 (t, J = 7.8 Hz, 2H), 2.26 (s, 3H), 1.58−1.55 (m, 2H), 1.26 (m, 24H), 0.89 (t, J = 6.3 Hz, 3H). ^{13}C NMR (75,47 MHz, $CDCl_3$, ppm) δ 169.2, 167.3, 148.3, 143.0, 130.7, 127.3, 126.3, 120.4, 52.3, 34.9, 32.1, 31.5, 29.8−29.5, 22.8, 20.9, 14.2. HRMS (ESI+): m/z [(M + H)$^+$] calcd for $C_{25}H_{40}O_4$: 405.2999, found 405.2997.

*3-Pentadecylphenol (**9**, LDT10).* To a solution of 10.0 g of the mixture of **2** (∼33.0 mmol) in ethanol (30 mL) was added 0.2 g of 10% of palladium on carbon (2 mol %), and the mixture was shaken in a Parr apparatus, under hydrogen atmosphere (60 psi) for 4 h. Then, the reaction mixture was filtered in a sintered funnel. The solvent was evaporated under reduced pressure and the residue was purified by chromatography (silica gel, hexane/dichloromethane 1:1) to afford **9** as a white solid. Yield 90% (9.1 g, 29.7 mmol). HPLC purity: 99%. mp 50−53 °C. IR (KBr, cm^{-1}): 3337, 2916, 2848, 1592, 1458. ^1H NMR (500.13 MHz, $CDCl_3$, ppm) δ 7.16 (dd, J = 7.8, 7.4 Hz, 1H), 6.78 (d, J = 7.4 Hz, 1H), 6.69 (br s, 1H), 6.68 (d, J = 7.8 Hz, 1H), 2.58 (t, J = 7.8 Hz, 2H), 1.62−1.60 (m, 2H), 1.33−1.29 (m, 24H), 0.92 (t, J = 6.8 Hz, 3H). ^{13}C NMR (125.66 MHz, $CDCl_3$, ppm) δ 155.6, 145.2, 129.6, 121.2, 115.6, 112.7, 36.0, 32.2, 31.5, 29.9−29.6, 22.9, 14.3. HRMS (ESI+): m/z [(M + H)$^+$] calcd for $C_{21}H_{36}O$: 305.2839, found 305.2833.

*2-Hydroxy-4-pentadecylbenzaldehyde (**10**, LDT77).* Compound **9** (5.0 g, 16.4 mmol) was dissolved in THF (180 mL) followed by the addition of triethylamine (32.8 mmol), $MgBr_2$ (32.8 mmol), and *p*-formaldehyde (49.3 mmol). The reaction mixture was refluxed under nitrogen for 24 h. Then, the mixture was concentrated under reduction pressure and extracted with ethyl ether (3 × 50 mL). The combined organic fractions were washed with a 10% hydrochloric solution (2 × 15 mL) and brine (30 mL) and dried with anhydrous sodium sulfate. The solvent was evaporated under reduced pressure, and the product was purified by chromatography (silica gel) using a gradient of a mixture hexane/dichloromethane (5:1) to afford **10** as a white solid. Yield 90% (4.9 g, 14.8 mmol). mp 48−50 °C. IR (KBr, cm^{-1}): 2918, 2850, 1671, 1629, 1570, 1472, 1390, 1193, 1227. ^1H NMR (300.13 MHz, $CDCl_3$, ppm) δ 11.05 (s, 1H, OH), 9.83 (s, 1H), 7.44 (d, J = 7.8 Hz, 1H), 6.83 (dd, J = 8.5, 1.4 Hz, 1H), 6.81 (s, 1H), 2.62 (t, J = 7.7 Hz, 2H), 1.65−1.60 (m, 2H), 1.30−1.26 (m, 24H), 0.89 (t, J = 6.6 Hz, 3H). ^{13}C NMR (75,47 MHz, $CDCl_3$, ppm) δ 196.0, 162.0, 154.0, 133.8, 120.7, 119.1, 117.3, 36.6, 32.1, 30.9, 29.9−29.4, 22.9, 14.3.

*2-Methoxy-4-pentadecylbenzaldehyde (**11**, LDT220).* Compound **10** (3.0 g, 9.0 mmol) was dissolved in acetone (50 mL), followed by the addition of K_2CO_3 (18.0 mmol). The reaction mixture was stirred for 20 min, and then methyl iodide (36.0 mmol) was added. The reaction was refluxed at 120 °C for 20 h. The mixture was then concentrated under reduced pressure and extracted with dichloromethane (2 × 40 mL). The organic phase was washed with a 10% hydrochloric solution (2 × 15 mL) and brine (20 mL) and dried with anhydrous sodium sulfate. The solvent was evaporated under reduced pressure, and the product was purified by chromatography (silica gel), using a gradient of a mixture hexane/dichloromethane (2:5) to afford **11** as a white solid. Yield 80% (2.5 g, 7.2 mmol). mp 39−41 °C. IR (KBr, cm^{-1}): 2923, 2851, 1675, 1605, 1477, 1267, 1204, 1161. ^1H NMR (300.13 MHz, $CDCl_3$, ppm) δ 10.40 (s, 1H, CHO), 7.74 (d, J = 7.9 Hz, 1H), 6.85 (d, J = 7.9 Hz, 1H), 6.78 (s, 1H), 3.92 (s, 3H, OCH_3), 2.64 (t, J = 7.7 Hz, 2H), 1.31−1.26 (m, 24H), 1.66−1.61 (m, 2H), 0.88 (t, J = 6.6 Hz, 3H). ^{13}C NMR (75,47 MHz, $CDCl_3$, ppm) δ 189.6, 162.1, 152.6, 128.8, 123.1, 121.2, 111.7, 55.7, 36.9, 32.1, 31.2, 29.9−29.5, 22.9, 14.3.

*2-Hydroxy-4-pentadecylbenzoic Acid (**12**, LDT380) and 2-Methoxy-4-pentadecylbenzoic Acid (**14**, LDT407).* Compound **10** or **11** (1.0 mmol) was dissolved in the mixture of dichloromethane (10 mL) and DMSO (10 mL). To the solution, cooled in an ice/water bath, was added sodium chlorite solution 1 M (5 mL) and, carefully, sodium monophosphate solution 1 M (5 mL). The mixture was stirred at room temperature for 16 h. Then, the mixture was extracted with ethyl acetate (20 mL—for **12**) or dichloromethane (20 mL—for **14**), washed with 10% hydrochloric solution (10 mL) and brine solution (10 mL) and dried over anhydrous sodium sulfate. After removal of the solvent at reduced pressure, the residue was

https://doi.org/10.1021/acs.jmedchem.1c01542
J. Med. Chem. 2022, 65, 1961−1978

purified by recrystallization from dichloromethane/hexane (1:5) (for **12**) or by column chromatography (for **14**) containing silica gel eluted with a dichloromethane/hexane mixture (3:5) to afford the respective acids.

*2-Hydroxy-4-pentadecylbenzoic Acid (**12**, LDT380).* White solid. Yield 89% (0.3 g, 0.9 mmol). HPLC purity: 96%. mp 92−94 °C. IR (KBr, cm^{-1}): 2919, 2850, 1654, 1499, 1458, 1256, 1221. ^1H NMR (300.13 MHz, Py-d_5, ppm) δ 11.04 (s, 1H, OH), 8.25 (d, J = 8.0 Hz, 1H), 7.13 (s, 1H), 6.83 (dd, J = 7.6, 1.4 Hz, 1H), 2.63 (t, J = 7.6 Hz, 2H), 1.67−1.63 (m, 2H), 1.37−1.24 (m, 24H), 0.89 (t, J = 6.6 Hz, 3H). ^{13}C NMR (75,47 MHz, $CDCl_3$, ppm) δ 174.9, 163.5, 151.9, 131.6, 120.2, 117.8, 113.2, 36.8, 32.6, 31.7, 30.5−30.0, 23.4, 14.8. HRMS (ESI-TOF): m/z $[(M - H)^+]$ calcd for $C_{22}H_{36}O_3$: 347.2585, found 347.2581.

*2-Methoxy-4-pentadecylbenzoic Acids (**14**, LDT407).* White solid. Yield 92% (0.3 g, 0.9 mmol). HPLC purity: 98%. mp 73−75 °C. IR (KBr, cm^{-1}): 2917, 2850, 1718, 1611, 1466, 1420, 1252, 1175, 1033. ^1H NMR (300.13 MHz, $CDCl_3$, ppm) δ 8.07 (d, J = 8.0 Hz, 1H), 6.95 (d, J = 7.9 Hz, 1H), 6.85 (s, 1H), 4.07 (s, 3H, OCH_3), 2.66 (t, J = 7.7 Hz, 2H), 1.63−1.62 (m, 2H), 1.32−1.26 (m, 24H), 0.88 (t, J = 6.7 Hz, 3H). ^{13}C NMR (75.47 MHz, $CDCl_3$, ppm) δ 165.7, 158.3, 151.7, 133.9, 122.6, 115.2, 111.8, 56.7, 36.5, 32.1, 31.2, 29.9−29.5, 22.9, 14.3. HRMS (ESI+): m/z $[(M + H)^+]$ calcd for $C_{23}H_{38}O_3$: 363.2894, found 363.2903.

*Methyl 2-Hydroxy-4-pentadecylbenzoate (**15**, LDT381) and Methyl 2-Methoxy-4-pentadecylbenzoate (**17**, LDT382).* **12** or **14** (3.0 mmol) was dissolved in methanol (30 mL). To the solution, cooled in an ice/water bath, concentrated H_2SO_4 (1 mL) was carefully added, and the reaction was stirred under reflux for 16 h. Then, the solvent was removed under reduced pressure and the obtained mixture was extracted with dichloromethane (25 mL), washed with distilled water (10 mL) and brine (10 mL), and dried over anhydrous sodium sulfate. The solvent was evaporated under reduced pressure, and the product was purified by chromatography containing silica gel, eluted with a mixture of dichloromethane/hexane (2:5), to afford the respective methyl esters.

*Methyl 2-Hydroxy-4-pentadecylbenzoate (**15**, LDT381).* White solid. Yield 95% (1.1 g, 2.9 mmol). HPLC purity: 96%. mp 41−43 °C. IR (KBr, cm^{-1}): 2917, 2849, 1686, 1566, 1501, 1472, 1444, 1260, 1204, 1155. ^1H NMR (500.13 MHz, $CDCl_3$, ppm) δ 10.72 (s, 1H, OH), 7.73 (d, J = 8.1 Hz, 1H), 6.81 (s, 1H), 6.71 (d, J = 7.2 Hz, 1H), 3.94 (s, 3H, OCH_3), 2.59 (t, J = 7.6 Hz, 2H), 1.62−1.60 (m, 2H), 1.31−1.27 (m, 24H), 0.89 (t, J = 6.6 Hz, 3H). ^{13}C NMR (125.66 MHz, $CDCl_3$, ppm) δ 170.8, 161.8, 152.2, 130.0, 120.0, 117.2, 110.2, 52.3, 36.4, 32.2, 30.9, 29.9−29.5, 22.9, 14.3. HRMS (ESI+): m/z $[(M + H)^+]$ calcd for $C_{23}H_{38}O_3$: 363.2894, found 363.2904.

*Methyl 2-Methoxy-4-pentadecylbenzoate (**17**, LDT382).* White solid. Yield 92% (1.0 g, 2.8 mmol). HPLC purity: 96%. mp 41−43 °C. IR (KBr, cm^{-1}): 2918, 2848, 1702, 1610, 1466, 1439, 1175, 1138, 1097, 1030. ^1H NMR (300.13 MHz, $CDCl_3$, ppm) δ 7.74 (d, J = 7.9 Hz, 1H), 6.80−6.77 (m, 2H), 3.90 (s, 3H, OCH_3), 3.87 (s, 3H, OCH_3), 2.62 (t, J = 7.7 Hz, 2H), 1.64−1.60 (m, 2H), 1.30−1.27 (m, 24H), 0.89 (t, J = 6.6 Hz, 3H). ^{13}C NMR (75.47 MHz, $CDCl_3$, ppm) δ 166.8, 159.6, 149.8, 132.0, 120.4, 117.4, 112.3, 56.1, 52.0, 36.5, 32.1, 31.2, 29.9−29.5, 22.9, 14.3. HRMS (ESI+): m/z $[(M + H)^+]$ calcd for $C_{24}H_{40}O_3$: 377.3050, found 377.3053.

*2-Acetoxy-4-pentadecylbenzoic Acid (**13**, LDT383) and 2-Acetoxy-4-pentadecylbenzoic Acid (**16**, LDT384).* Compound **12** or **15** (1.0 mmol), acetic anhydride (10.0 mmol), and phosphoric acid (three drops) were placed in an Erlenmeyer flask inside an unmodified household microwave oven and irradiated for 5 min (5 × 1′) at a power of 270 W. After the completion of the reaction, the mixture was extracted with ethyl acetate (15 mL) and washed with a solution of 5% sodium bicarbonate (20 mL), brine solution (20 mL), and dried over anhydrous sodium sulfate. The residue was concentrated under reduced pressure and purified by chromatography (silica gel, using a gradient of a mixture hexane/ethyl acetate) to afford final acetoxy derivatives.

*2-Acetoxy-4-pentadecylbenzoic Acid (**13**, LDT383).* White solid. Yield 80% (0.3 g, 0.8 mmol). HPLC purity: 98%. mp 103−105 °C. IR (KBr, cm^{-1}): 2916, 2849, 1763, 1685, 1448, 1202, 1163, 1084. ^1H NMR (500.13 MHz, Py-d_5, ppm) δ 8.40 (d, J = 7.9 Hz, 1H), 7.33−7.27 (m, 2H), 2.67 (t, J = 7.5 Hz, 2H), 2.54 (s, 3H), 1.68−1.60 (m, 2H), 1.39−1.26 (m, 24H), 0.92 (t, J = 7.0 Hz, 3H). ^{13}C NMR (125.66 MHz, Py-d_5, ppm) δ 171.1, 168.4, 152.6, 150.7, 133.4, 127.2, 124.9, 123.7, 36.5, 32.9, 31.9, 30.8−30.3, 23.7, 22.2, 15.1. HRMS (ESI +): m/z $[(M + NH_4)^+]$ calcd for $C_{24}H_{38}O_4$ 408.3108, found 408.3114.

*2-Acetoxy-4-pentadecylbenzoic Acid (**16**, LDT384).* White solid. Yield 88% (0.3 g, 0.9 mmol). HPLC purity: 97%. mp 53−55 °C. IR (KBr, cm^{-1}): 2916, 2849, 1764, 1721, 1618, 1435, 1206, 1146. ^1H NMR (500.13 MHz, $CDCl_3$, ppm) δ 7.94 (d, J = 8.0 Hz, 1H), 7.12 (br d, J = 7.4 Hz, 1H), 6.92 (s, 1H), 3.86 (s, 3H), 2.65 (t, J = 7.6 Hz, 2H), 2.35 (s, 3H), 1.69−1.58 (m, 2H), 1.39−1.24 (m, 24H), 0.89 (t, J = 7.0 Hz, 3H). ^{13}C NMR (125.66 MHz, Py-d_5, ppm) δ 170.0, 165.1, 151.0, 150.4, 131.9, 126.3, 123.8, 120.4, 52.2, 35.9, 32.1, 30.9, 29.9−29.4, 22.9, 21.2, 14.3. HRMS (ESI+): m/z $[(M + Na)^+]$ calcd for $C_{25}H_{40}O_4$: 405.2999, found 405.3006.

*3-Pentadecylphenol Acetate (**18**, LDT12).* Compound **9** (2.0 g, 6.6 mmol), acetic anhydride (13.0 mmol), and phosphoric acid (two drops) were placed in an Erlenmeyer flask inside an unmodified household microwave oven and irradiated for 3 min (3 × 1′) at a power of 400 W. After the completion of the reaction, the mixture was extracted with ethyl acetate (3 × 10 mL) and the organic phases together were washed with a solution of 5% sodium bicarbonate (20 mL) and brine solution (10 mL) and dried over anhydrous sodium sulfate. The residue was concentrated under reduced pressure and purified by chromatography (silica gel, hexane/dichloromethane 1:1) to provide **18** as a white solid. Yield 91% (2.0 g, 5.9 mmol). HPLC purity: 99%. mp 46−48 °C. IR (KBr, cm^{-1}): 3482, 2917, 2850, 1761, 1588, 1472, 1370, 1206, 1142, 1015. ^1H NMR (500.13 MHz, $CDCl_3$, ppm) δ 7.26 (dd, J = 8.1, 5.2 Hz, 1H), 7.03 (d, J = 7.6 Hz, 1H), 6.88 (m, 2H), 2.60 (t, J = 7.5 Hz, 5H), 2.27 (s, 3H), 1.60 (q, 2H), 1.31−1.26 (m, 24H), 0.88 (t, J = 6.5 Hz, 3H). ^{13}C NMR (125.66 MHz, $CDCl_3$, ppm) δ 169.7, 150.8, 144.9, 129.2, 126.1, 121.6, 118.8, 35.9, 32.1, 31.4, 29.9−29.5, 22.8, 21.3, 14.3. HRMS (ESI+): m/z $[(M + H)^+]$ calcd for $C_{23}H_{38}O_2$: 347.2945, found 347.2941.

*1-Methoxy-3-pentadecyl Benzene (**19**, LDT27).* Compound **9** (1.0 g, 3.3 mmol) was dissolved in acetone (20 mL), followed by the addition of potassium carbonate (6.6 mmol) and methyl iodide (8.2 mmol). The mixture was refluxed at 65 °C for 24 h. The solution was concentrated under reduced pressure, and the residue extracted with ether (3 × 20 mL). The combined organic phases were washed with 10% aqueous hydrochloric acid (20 mL) and brine (20 mL) and dried over anhydrous sodium sulfate. The solvent was evaporated under reduced pressure, and the residue was purified by chromatography (silica gel, hexane/dichloromethane 1:1), affording **19** as a colorless oil. Yield 80% (0.8 g, 2.6 mmol). HPLC purity: 99%. IR (film, cm^{-1}): 2923, 2852, 1601, 1584, 1488, 1465, 1259, 1047. ^1H NMR (300.13 MHz, $CDCl_3$, ppm) δ 7.22 (m, 1H), 6.80 (d, J = 7.7 Hz, 1H), 6.75 (d, J = 6.7 Hz, 2H), 3.82 (s, 3H), 2.60 (t, J = 7.8 Hz, 2H), 1.66−1.60 (m, 2H), 1.32−1.28 (m, 24H), 0.91 (t, J = 6.5 Hz, 3H).^{13}C NMR (75.47 MHz, $CDCl_3$, ppm) δ 159.8, 144.8, 129.3, 121.0, 114.4, 111.0, 55.3, 36.3, 32.2, 31.6, 29.9−29.6, 22.9, 14.3. HRMS (ESI+): m/z $[(M + H)^+]$ calcd for $C_{22}H_{38}O$: 319.2995, found 319.3010.

*Ethyl 2-(3-Pentadecylphenoxy)acetate (**20**, LDT15) and (Z)-Ethyl 2-(3-(Pentadec-8-en-1-yl)phenoxy)acetate (**24**, LDT486A).* Compound **9** or **2A** (4.5 mmol) was dissolved in acetone (30 mL), followed by the addition of potassium carbonate (11.2 mmol). The solution was stirred for 20 min, and then ethyl 2-bromoacetate (5.6 mmol) was added. The reaction mixture was kept under vigorous stirring at room temperature for 24 h. After reduction of the volume of the solvent under reduced pressure, the mixture was extracted with ethyl acetate (2 × 10 mL) and the combined organic fractions were washed with a 10% hydrochloric acid (10 mL) and brine (10 mL) and dried over anhydrous sodium sulfate. The solvent was evaporated under reduced pressure, and the residue was purified by chromatography (silica gel, hexane/dichloromethane 1:1), yielding the respective esters **20** and **24**.

https://doi.org/10.1021/acs.jmedchem.1c01542
J. Med. Chem. 2022, 65, 1961−1978

*Ethyl 2-(3-Pentadecylphenoxy)acetate (**20**, LDT15).* White solid. Yield 90% (1.6 g, 4.1 mmol). HPLC purity: 95%. mp 30−31 °C. IR (KBr, cm^{-1}): 2918, 2850, 1753, 1612, 1586, 1490, 1466, 1242, 1096. ^1H NMR (500.13 MHz, $CDCl_3$, ppm) δ 7.19 (t, J = 7.8 Hz, 1H), 6.81 (d, J = 7.5 Hz, 1H), 6.77 (br, 1H), 6.71 (dd, J = 8.1, 2.2 Hz, 1H), 4.61 (s, 2H), 4.28 (q, J = 7.1 Hz, 2H), 2.58 (t, J = 7.7 Hz, 2H), 1.62−1.57 (m, 2H), 1.32−1.30 (m, 27H), 0.89 (t, J = 6.9 Hz, 3H). ^{13}C NMR (125.66 MHz, $CDCl_3$, ppm) δ 169.2, 158.0, 145.0, 129.4, 122.1, 115.3, 111.6, 65.5, 61.5, 36.2, 32.1, 31.5, 29.9−29.5, 22.9, 14.4, 14.3. HRMS (ESI+): m/z [(M + H)$^+$] calcd for $C_{25}H_{42}O_3$: 391.3207, found 391.3202.

*(Z)-Ethyl 2-(3-(Pentadec-8-en-1-yl)phenoxy)acetate (**24**, LDT486A).* Colorless oil. Yield 90% (1.6 g, 4.1 mmol). HPLC purity: 98%. ^1H NMR (300.13 MHz, $CDCl_3$, ppm) δ 7.19 (m, 1H), 6.82 (d, J = 7.7 Hz, 1H), 6.77 (d, J = 6.7 Hz, 1H), 6.72 (dd, J = 8.1, 2.2 Hz, 1H); 5.47−5.34 (m, 2H); 4.61 (s, 2H); 4.27 (q, J = 7.1 Hz, 2H), 2.58 (t, J = 7.7 Hz, 2H), 2.03−2.01 (m 4H); 1.63−1.58 (m, 2H), 1.33−1.27 (m, 19H), 0.91−0.87 (m, 3H). ^{13}C NMR (75.47 MHz, $CDCl_3$, ppm) δ 169.3, 158.1, 145.0, 130.1−130.0, 129.4, 122.1, 115.3, 111.7, 65.7, 61.5, 36.2, 32.0, 31.5, 29.9−29.2, 27.4, 22.8, 14.4−14.3. HRMS (ESI+): m/z [(M + H)$^+$] calcd for $C_{25}H_{40}O_3$: 389.3011, found 389.3047.

*2-Methyl-2-(3-pentadecylphenoxy) Ethyl Propanoate (**21**, LDT408) and (Z)-Ethyl 2-Methyl-2-(3-(pentadec-8-en-1-yl)-phenoxy)propanoate (**25**, LDT539A).* Compound **9** or **2A** (2.9 mmol) was solubilized in acetonitrile (6 mL), followed by the addition of potassium carbonate (5.9 mmol) and potassium iodide (2.9 mmol). The mixture was stirred for 20 min, and then ethyl α-bromoisobutyrate (8.9 mmol) was added. The reaction was heated at 82 °C for 24 h. After reduction of the volume of the solvent, the mixture was extracted with ether (2 × 10 mL) and the combined organic fractions were washed with 10% aqueous hydrochloric acid (10 mL) and brine solution (10 mL) and dried over sodium sulfate. The solvent was evaporated under reduced pressure, and the residue was purified by chromatography (silica gel, dichloromethane/chloroform 1:1) affording the respective esters **21** and **25**.

*2-Methyl-2-(3-pentadecylphenoxy) Ethyl Propanoate (**21**, LDT408).* Pale-yellow oil. Yield 92% (1.1 g, 2.7 mmol). HPLC purity: 97%. IR (film, cm^{-1}): 2925, 2854, 1735, 1602, 1466, 1142, 1025. ^1H NMR (300.13 MHz, $CDCl_3$, ppm) δ 7.13 (t, J = 7.8 Hz, 1H), 6.81 (d, J = 7.5 Hz, 1H), 6.70 (br, 1H), 6.65 (dd, J = 8.1, 1.7 Hz, 1H), 4.24 (q, J = 7.1 Hz, 2H), 2.55 (t, J = 7.7 Hz, 2H), 1.60−1.57 (m, 8H), 1.28−1.24 (m, 27H), 0.89 (t, J = 6.7 Hz, 3H). ^{13}C NMR (75.47 MHz, $CDCl_3$, ppm) δ 174.6, 155.6, 144.7, 128.9, 122.5, 119.6, 116.3, 79.1, 61.5, 36.1, 32.1, 31.5, 29.9−29.5, 25.6, 22.9, 14.3. HRMS (ESI+): m/z [(M + H)$^+$] calcd for $C_{27}H_{46}O_3$: 419.3520, found 419.3521.

*(Z)-Ethyl 2-Methyl-2-(3-(pentadec-8-en-1-yl)phenoxy)-propanoate (**25**, LDT539A).* Colorless oil. Yield 86% (1.0 g, 2.5 mmol). HPLC purity: 97%. ^1H NMR (300.13 MHz, $CDCl_3$, ppm) δ 7.17 (t, J = 7.8 Hz, 1H), 6.84 (d, J = 7.5 Hz, 1H), 6.73 (s, 1H), 6.69 (dd, J = 8.2, 1.9 Hz, 1H); 5.41−5.37 (m, 2H); 4.28 (q, J = 7.1 Hz, 2H), 2.58 (t, J = 7.7 Hz, 2H), 2.07−1.98 (m, 4H); 1.64−1.61 (m, 8H), 1.38−1.27 (m, 19H), 0.95−0.91 (m, 3H). ^{13}C NMR (75.47 MHz, $CDCl_3$, ppm) δ 174.6, 155.6, 144.4, 130.1−130.0, 128.9, 122.5, 119.6, 116.3, 79.1, 61.5, 36.1, 31.4−30.1, 29.9−29.2, 27.4, 22.8, 14.3−14.0. HRMS (ESI+): m/z [(M + H)$^+$] calcd for $C_{27}H_{44}O_3$: 417.3324, found 417.3363.

*2-(3-Pentadecylphenoxy) Acetic Acid (**22**, LDT16), 2-Methyl-2-(3-pentadecylphenoxy) Propanoic Acid (**23**, LDT409), (Z)-2-(3-(Pentadec-8-en-1-yl)phenoxy) Acetic Acid (**26**, LDT487A), and (Z)-2-Methyl-2-(3-(pentadec-8-en-1-yl)phenoxy)propanoic Acid (**27**, LDT540A).* Compound **20**, **21**, **24**, or **25** (1.0 mmol) was dissolved in tetrahydrofuran (5.0 mL), and a solution of lithium hydroxide (4.0 mmol) in distilled water (2 mL) was added, followed by phase transfer catalyst Aliquat (four drops). The mixture was kept under vigorous stirring at room temperature (for **20** and **24**) or heated at 65 °C (for **21** and **25**) for 4 h. Then, the mixture was acidified with concentrated hydrochloric acid to pH 1, and it was extracted with ethyl acetate (3 × 10 mL). The combined organic fractions were washed with brine (10 mL) and dried with sulfate anhydrous sodium. The solvent was evaporated under reduced pressure, and the residue was purified by chromatography (silica gel, using a gradient of a mixture chloroform/ethanol), affording the respective acids.

*2-(3-Pentadecylphenoxy) Acetic Acid (**22**, LDT16):* White solid. Yield 90% (0.3 g, 0.9 mmol). HPLC purity: 99%. mp 77−79 °C. IR (KBr, cm^{-1}): 2956, 2849, 1733, 1611, 1577, 1470, 1458, 1273. ^1H NMR (500.13 MHz, $CDCl_3$, ppm) δ 7.21 (t, J = 7.7 Hz, 1H), 6.85 (d, J = 7.4 Hz, 1H), 6.78 (s, 1H), 6.73 (d, J = 8.0 Hz, 1H), 4.68 (s, 2H), 2.58 (t, J = 7.6 Hz, 2H), 1.60−1.59 (m, 2H), 1.30−1.26 (m, 24H), 0.89 (t, J = 6.5 Hz, 3H). ^{13}C NMR (125.66 MHz, $CDCl_3$, ppm) δ 173.7, 157.5, 145.2, 129.6, 122.6, 115.3, 111.6, 65.0, 36.1, 32.1, 31.5, 29.9−29.5, 22.9, 14.3. HRMS (ESI+): m/z [(M + H)$^+$] calcd for $C_{23}H_{38}O_3$: 363.2894, found 363.2898.

*2-Methyl-2-(3-pentadecylphenoxy) Propanoic Acid (**23**, LDT409).* White solid. Yield 90% (0.3 g, 0.9 mmol). HPLC purity: 98%. mp 46−48 °C. IR (KBr, cm^{-1}): 2920, 2850, 1702, 1611, 1583, 1488, 1469, 1166. ^1H NMR (300.13 MHz, $CDCl_3$, ppm): 7.17 (t, J = 7.8 Hz, 1H), 6.89 (d, J = 7.6 Hz, 1H), 6.79−6.74 (m, 2H), 2.57 (t, J = 7.7 Hz, 2H), 1.62 (m, 8H), 1.28 (s, 24H), 0.90 (t, J = 6.6 Hz, 3H); ^{13}C NMR (75.47 MHz, $CDCl_3$, ppm) δ 179.2, 154.7, 144.8, 129.1, 123.6, 121.0, 117.6, 79.6, 36.0, 32.1, 31.5, 29.9−29.5, 25.3, 22.9, 14.3. HRMS (ESI+): m/z [(M + H)$^+$] calcd for $C_{25}H_{42}O_3$: 391.3207, found 391.3213.

*(Z)-2-(3-(Pentadec-8-en-1-yl)phenoxy) Acetic Acid (**26**, LDT487A).* White solid. Yield 88% (0.3 g, 0.9 mmol). HPLC purity: 97%. mp 52−54 °C. ^1H NMR (300.13 MHz, $CDCl_3$, ppm) δ 7.21 (d, J = 7.8 Hz, 1H), 6.85 (d, J = 7.55 Hz, 1H), 6.78 (s, 1H), 6.73 (dd, J = 8.2, 2.2 Hz, 2H), 5.38−5.34 (m, 2H), 4.68 (s, 2H), 2.59 (t, J = 7.7 Hz, 2H), 2.03−2.00 (m 4H), 1.61 (m, 2H), 1.32−1.28 (m, 15H), 0.92−0.87 (m, 3H). ^{13}C NMR (75.47 MHz, $CDCl_3$, ppm) δ 174.1, 157.7, 145.2, 130.1−130.0, 129.5, 122.5, 115.3, 111.6, 61.5, 36.1, 32.0, 31.5, 29.9−29.2, 27.4, 22.8, 14.3. HRMS (ESI+): m/z [(M + H)$^+$] calcd for $C_{23}H_{36}O_3$: 361.2744, found 361.2741.

*(Z)-2-Methyl-2-(3-(pentadec-8-en-1-yl)phenoxy) Propanoic Acid (**27**, LDT540A).* Colorless oil. Yield 80% (0.3 g, 0.8 mmol). HPLC purity: 98%. ^1H NMR (300.13 MHz, $CDCl_3$, ppm) δ 7.18 (t, J = 7.8 Hz, 1H), 6.91 (d, J = 7.5 Hz, 1H), 6.77−6.74 (m, 2H), 5.37−5.33 (m, 2H), 2.57 (t, J = 7.7 Hz, 2H), 2.03−2.02 (m, 4H), 1.60 (m, 8H), 1.30−1.26 (m, 19H), 0.89−0.86 (m, 3H). ^{13}C NMR (75.47 MHz, $CDCl_3$, ppm) δ 177.2, 154.2, 144.8, 130.3−130.0, 129.2−128.2, 124.0, 122.4, 121.4, 118.0, 80.0, 36.0, 32.0, 31.5, 30.0−29.2, 27.4, 25.2, 22.9, 14.3. HRMS (ESI+): m/z [(M + H)$^+$] calcd for $C_{25}H_{40}O_3$: 389.3011, found 389.3051.

Luciferase Assays. Human embryonic kidney (HEK293) cells were maintained in Dulbecco's modified Eagle's medium supplemented with 10% fetal bovine serum (FBS). Cell transfection was performed in media containing 10% charcoal-stripped fetal bovine serum using calcium phosphate in 96-well plates. The total amount of plasmid DNA (150 ng/well) included 50 ng of UAS-luciferase reporter, 20 ng of β-galactosidase, 15 ng of nuclear receptor (GAL4-hPPARα, GAL4-hPPARγ, and GAL4-hPPARδ), and pGEM filler plasmid. Ligands were added 6−8 h post transfection. Cells were harvested 14−16 h after ligand addition and were assayed for luciferase and β-galactosidase activity to control for transfection efficiency.

Primary Hepatocytes. Mouse primary hepatocytes were isolated by collagenase perfusion as previously described.[50] Cells were plated onto type I collagen-coated plates at 0.5 × 10^6 cells per well for 2 h in attachment media (William's E Media, 10% charcoal-stripped FBS, 1× penicillin/streptomycin, and 10 nM insulin) and then switched to overnight media (M199 media, 5% charcoal-stripped FBS, 1× penicillin/streptomycin, and 1 nM insulin). Ligand treatments were carried out on the following day in M199 media without FBS. The cells were harvested 16 h later for RNA extraction.

3T3-L1 Adipocyte Differentiation Assays. 3T3-L1 cells were maintained in Dulbecco's modified Eagle's medium supplemented with 10% fetal calf serum. Adipocyte differentiation was induced in 2-day post-confluent cells by treating the cells with 100 μg/mL isobutylmethylxanthine, 1 μM dexamethasone, and 5 μg/mL insulin with 10% FBS in DMEM (day 0). Rosiglitazone and CNSL

https://doi.org/10.1021/acs.jmedchem.1c01542
J. Med. Chem. 2022, 65, 1961−1978

derivatives were added at the start of differentiation. Two days later, the cells were switched to fresh medium containing 5 μg/mL insulin with 10% FBS. After an additional 72 h, the cells were switched to maintenance media containing 10% FBS in DMEM. Thereafter, the media was changed every 2 days. The cells were harvested on day 11 for RNA expression, and Oil Red O staining was used to estimate lipid accumulation.

Oil Red O Staining. Following 11 days of differentiation, the cells were washed with PBS twice and fixed in 10% neutral buffered formalin (Sigma) for 1 hr at room temperature, followed by two double-distilled H_2O (ddH_2O) and two washes with 60% isopropanol. The cells were then stained with 0.6% (w/v) Oil Red O solution (60% isopropanol, 40% water) for 10 min at room temperature, followed by five washes with double-distilled H_2O to remove unbound dye, and images were taken with a Leica M205 FA microscope.

RNA Isolation, cDNA Synthesis, and Real-Time Quantitative PCR (QPCR) Analysis. Total RNA was extracted from cells using RNA STAT-60 (Tel-Test Inc.), followed by DNase I treatment (RNase-free; Roche), and reverse-transcribed into cDNA with random hexamers using the High Capacity Reverse Transcription System (ABI; Applied Biosystems). QPCR analysis was performed on an ABI 7900 in 384-well plates using 2× SYBR Green PCR Master Mix (ABI). Relative mRNA levels were calculated using the comparative Ct method normalized to 36B4 mRNA for primary adipocytes and cyclophilin mRNA for differentiated 3T3-L1 adipocytes.

Compound Screening in Transgenic Zebrafish Line. Ligands were screened in human PPARα, PPARγ, and PPARδ-expressing zebrafish lines. One day post-fertilization PPARα, PPARγ, and PPARδ heterozygous embryos were heat-shocked at 37 °C for 30 min, dechorionated, and then arrayed. Embryos were maintained in embryo water, including 0.075 g/L $NaHCO_3$, 0.018 g/L sea salt, and 0.0084 g/L $CaSO_4{\cdot}2H_2O$. Before ligand incubation, the embryo water was replaced with fresh embryo water supplemented with CNSL derivatives. The CNSL derivatives were screened at EC_{50}'s. Embryos were incubated at 28 °C for 14 h in the presence of ligands, anesthetized with Tricaine (Sigma), and imaged for GFP fluorescence using an ImageXpress Velos laser scanning cytometer.

Liver Microsome Stability Assays. Metabolic stability assays were performed by incubating the CNSL derivatives with mouse liver microsomes. Briefly, 1 μL of 1 mM ligands was incubated with NADPH producing system (100 μL of 50 U/mL isocitrate dehydrogenase, 25 μL of 0.1 M $MgCl_2$, and 25 μL of 0.1 M DL-isocitrate trisodium salt), 324 μL of 0.1 M K^+ phosphate buffer, and 12.5 μL of 3.3 mg/100 μL NADPH. The reaction was incubated at 37 °C for 5 min before 12.5 μL of 20 mg/mL B6C3F1 mouse microsomes (Thermo Fisher) was added. CNSL derivatives (**20**, **21**, **23**, and **27**) were incubated at 37 °C for desired time points (0 and 120 min) except **4** that was incubated for indicated time points (0, 2.5, and 5 min). At each time point, the reaction was quenched with 1 mL of methyl-*tert*-butyl ether (MTBE) and the mixture was vortexed for 3 min at room temperature. Once all of the time points were collected, the samples were centrifuged at 21 130*g* at room temperature for 3 min. The tubes were put in an ice bath (consisting of dry ice and isopropanol) to freeze the bottom layer. The top layer was poured into a 5 mL brown glass vial and dried under nitrogen gas. Samples were resuspended in 250 μL of HPLC-grade methanol prior to LC/MS/MS analysis. The disappearance of the parent compound (measured by changes in compound peak area/internal standard peak area) was plotted as the natural logarithm with respect to time to obtain the rate of disappearance, k (the slope of the line). Half-life ($t_{1/2}$) was calculated using the equation $\ln 2/k$.

Pharmacokinetic (PK) Study. Wild-type (WT) male C57Bl/6 mice (7−10 months old; $n = 4$ per two time points) were treated with **23** (LDT409) at 40 mg/kg, IP. The compound was administered in a solution of 5% DMSO, 5% Tween-80, and 90% saline. Four mice were sampled per time point and each animal was sampled twice, first by saphenous vein at 0.08, 0.16, 0.33, and 0.5 h, and next by terminal collection (trunk blood by decapitation) at 1, 2, 4, and 6 h. In a separate cohort of WT male C57Bl/6 mice, **23** was orally administered at 100 mg/kg in peanut butter pellets. Mice were acclimated to the peanut butter pellets (without drug) for 7 consecutive days, after which time the peanut butter pellets were consumed in less than 1 min. Twenty mice were used for the oral PK study with $n = 4$ per time point. Blood collection was performed by saphenous vein at 0.25, 0.5, 1, 1.5, and 2 h after drug administration, followed by the second terminal collection at 4, 8, 16, 24, and 38 h after administration. Plasma was obtained by centrifugation of blood at 500*g* at 4 °C for 20 min and stored at −80 °C. Plasma samples (50 μL) and standards were extracted with 250 μL of methanol containing the internal standard **4**, vortexed, and centrifuged at 21 130*g* at 4 °C for 5 min. The supernatant was transferred to autosampler vials for LC-MS/MS analysis.

LC-MS/MS Analysis. Samples from liver microsome stability assays and plasma samples from pharmacokinetics were analyzed by LC-MS/MS using a 6410 Triple Quadrupole instrument (Agilent Technologies, Santa Clara, CA) with electrospray ionization. Positive-ion mode was used for compounds **20** and **21**, and negative-ion mode for compounds **4**, **23**, and **27**. Samples were separated on a C18 column (Zorbax XDB, 4.6 × 50 mm^2, 3.5 μm) at a flow rate of 0.4 mL/min. Column temperature was set at 40 °C and injection volume was 10 μL. For positive-ion mode, the mobile phases consisted of HPLC-grade water (A) and MeOH (B), both containing 5 mM ammonium acetate. The following gradient was run: 0−1 min, 90% B; 1−3.3 min, 90−100% B; 3.3−7 min, 100% B; 7−14 min, 100% B; 14−14.1 min, 90% B. MS parameters were as follows: gas temperature 350 °C, nebulizer pressure 35 psi, drying gas (nitrogen) 10 L/min, VCap 4000 V, and fragmentor voltage 135 V. MS parameters monitoring for MRM transitions as follows: **20** (m/z 408.3→391.3, retention time: 10.2 min) and **21** (m/z 436.3→419.3, retention time: 12.0 min).

For negative-ion mode, the mobile phases consisted of HPLC-grade water (A) and acetonitrile (B), both containing 1% formic acid. The following gradient was run: 0−1 min, 90% B; 1−3.3 min, 90% to 100% B; 3.3−7 min, 100% B; 7−15 min, 100% B. The column was reequilibrated to initial conditions for 5.5 min. MS parameters were as follows: gas temperature 350 °C, nebulizer pressure 35 psi, drying gas (nitrogen) 10 L/min, VCap −4000 V, and fragmentor voltage 108 V. MS parameters monitoring for MRM transitions as follows: **4** (m/z 389 → 303.2 (retention time: 11.3 min)), **23** (m/z 389 → 303.2 (retention time: 7.4 min)) and **27** (m/z 387 → 301.2 (retention time: 9.2 min)).

Thermal Shift Assays. An Optim 1000 instrument (Unchained Labs) was used to record static light scattering signals during a temperature ramp using laser excited light at a wavelength of 473 nm. Changes in light scattering intensity reflect changes in aggregate size. Samples (9 μL) at a protein concentration of 1 mg/mL (~25 μM) were heated in 0.5 °C increments from 25 to 70 °C. The heating rate between temperature intervals was set to 1 °C/min. A typical temperature scan took two and a half minute including 30 s for thermal equilibration. All measurements were done in duplicate.

Molecular Docking. All compounds have been docked with Glide (Schrödinger, Inc.) into crystal structures of the ligand-binding domains of PPARα (PDB 2P54, 1.79 Å, co-crystallized with SRC1 peptide and **GW590735**), PPARγ (PDB 3U9Q, 1.52 Å, complexed with decanoic acid and PGC-1α peptide), and PPARδ (PDB 3D5F, 2.2 Å, complexed with 2-(4-(3-(4-acetyl-3-hydroxy-2-propylphenoxy)propoxy)phenoxy)acetic acid (**L41**)).

The protein structures were prepared using the Protein Prep wizard in Maestro by assigning bond orders using CCD database, adding hydrogens and filling in missing side chains using Prime. For side chains with multiple occupancies, the highest occupancy state was chosen. Protonation states for the co-crystallized ligands were generated at pH = 7 ± 2. The orientation of the water molecules; side chains of glutamines and asparagines, tautomers, and protonation states of histidines were sampled; and the hydrogens of the altered species were minimized. The protonation states of the protein side chains were assigned with PropKa at pH 7. Waters with less than three H-bonds to nonwaters were deleted. At the end, the protein

https://doi.org/10.1021/acs.jmedchem.1c01542
J. Med. Chem. 2022, 65, 1961−1978

underwent a hydrogen-only energy minimization using the OPLS3 force field.

During the protein GRID preparation, keeping in mind the largely elongated binding site, the binding site box was elongated in one direction to accommodate ligands with length up to 25 Å. Terminal hydroxyls and thioalcohols of C275, C276, T279, S280, Y314, and Y464 in PPARα; C285, S289, Y327, and Y473 in PPARγ; and C249, T252, T253, and Y437 in PPARδ were kept rotatable during the docking process. Possible H-bond constraints to side chains of Y314, H440, and Y464 in PPARα; H323, H449, Y473, and S289 in PPARγ; and H287 and H413 in PPARδ were set up but not used during the docking stage.

All ligands were prepared with LigPrep procedure using default settings, ionized to pH 7 ± 2, and energy-minimized using the OPLS3 force field.

The ligand docking was done using both Glide SP and XP scoring functions with flexible ligand sampling, and no constraints used, with 100 poses included for the post-docking minimization. Ten poses for each ligand were saved and viewed with Pose Viewer to allow visualization of flexible hydroxyls and thioalcohols.

Molecular Dynamics Simulations. To investigate stability of the key H-bonds formed by the polar warhead of **23**, we conducted molecular dynamics simulations using Desmond (D. E. Shaw Research, a part of the Schrödinger's Drug Discovery suite) using NPT ensembles at 310 K constant temperature and 1 atm constant pressure using the OPLS3 force field. A simulated box of 10 Å^3 was set up around the protein and filled with water molecules (SPC water model). Excessive charges were neutralized to make the total net formal charge of the system equal to 0, and 0.15 M NaCl was added to the buffer. The Nosé−Hoover chain thermostat was used to keep the temperature constant, and the Martyna−Tobias−Klein barostat was used to keep the system pressure constant. A nonbonding cutoff of 9.0 Å was used for Coulombic interactions, which is the electrostatic interactions between electric. A 2 fs time step was used, and a trajectory frame was saved every 5 ps. The total simulation time was 10 ns for each of the PPAR isoforms. Distances for key H-bonding, $\pi-\pi$, and cation$-\pi$ interactions were tracked during the simulations and analyzed afterward.

Statistical Analysis. Data handling, analysis, and graphical representations were performed using GraphPad 8.0 software (GraphPad, San Diego, CA). Statistical differences were determined by one-way analysis of variance followed by Holm−Šidák; $P < 0.05$ was accepted as statistically significant.

■ ASSOCIATED CONTENT

Supporting Information

The Supporting Information is available free of charge at https://pubs.acs.org/doi/10.1021/acs.jmedchem.1c01542.

Molecular formula strings (CSV)

QPCR primer sequences; dose−response curves of PPAR-active CNSL derivatives demonstrate many dual PPARα/PPARγ agonists with low micromolar affinities; docking of **23** with Glide SP scoring function in PPAR isoforms: general view; statistical analysis of key interactions of compound **23** with the three PPAR isoforms; ^{1}H NMR, and ^{13}C NMR spectra; HRMS spectra; compound purity and HPLC traces (PDF)

Docking models for **23** (LDT409) with PPARα (PDB)

Docking models for **23** (LDT409) with PPARδ (PDB)

Docking models for **23** (LDT409) with PPARγ (PDB)

■ AUTHOR INFORMATION

Corresponding Authors

Carolyn L. Cummins − *Department of Pharmaceutical Sciences, Leslie Dan Faculty of Pharmacy, University of Toronto, Toronto, Ontario M5S 3M2, Canada;* orcid.org/0000-0001-7603-6577; Phone: (416) 946-3466; Email: carolyn.cummins@utoronto.ca; Fax: (416) 978-8511

Luiz A. S. Romeiro − *Department of Pharmacy, Faculty of Health Sciences, University of Brasilia, Brasilia, DF 71910-900, Brazil;* orcid.org/0000-0001-5679-0820; Phone: (61) 3107-1620; Email: luizromeiro@unb.br

Authors

Cigdem Sahin − *Department of Pharmaceutical Sciences, Leslie Dan Faculty of Pharmacy, University of Toronto, Toronto, Ontario M5S 3M2, Canada*

Lilia Magomedova − *Department of Pharmaceutical Sciences, Leslie Dan Faculty of Pharmacy, University of Toronto, Toronto, Ontario M5S 3M2, Canada*

Thais A. M. Ferreira − *Department of Pharmacy, Faculty of Health Sciences, University of Brasilia, Brasilia, DF 71910-900, Brazil*

Jiabao Liu − *Donnelly Centre for Cellular and Biomolecular Research, University of Toronto, Toronto, Ontario M5S 3E1, Canada*

Jens Tiefenbach − *Donnelly Centre for Cellular and Biomolecular Research, University of Toronto, Toronto, Ontario M5S 3E1, Canada*

Priscilla S. Alves − *Department of Pharmacy, Faculty of Health Sciences, University of Brasilia, Brasilia, DF 71910-900, Brazil*

Fellipe J. G. Queiroz − *Department of Pharmacy, Faculty of Health Sciences, University of Brasilia, Brasilia, DF 71910-900, Brazil*

Andressa S. de Oliveira − *Department of Pharmacy, Faculty of Health Sciences, University of Brasilia, Brasilia, DF 71910-900, Brazil*

Mousumi Bhattacharyya − *Ontario Institute for Cancer Research, Toronto, Ontario M5G 0A3, Canada*

Julie Grouleff − *Ontario Institute for Cancer Research, Toronto, Ontario M5G 0A3, Canada*

Patrícia C. N. Nogueira − *CENAUREMN, Federal University of Ceará, Fortaleza, CE 60020-181, Brazil*

Edilberto R. Silveira − *CENAUREMN, Federal University of Ceará, Fortaleza, CE 60020-181, Brazil*

Daniel C. Moreira − *Faculty of Medicine, University of Brasilia, Brasilia, DF 71910-900, Brazil;* orcid.org/0000-0003-1961-7281

José Roberto Souza de Almeida Leite − *Faculty of Medicine, University of Brasilia, Brasilia, DF 71910-900, Brazil;* orcid.org/0000-0002-1096-3236

Guilherme D. Brand − *Chemistry Institute, University of Brasília, Brasília, DF 70910-900, Brazil;* orcid.org/0000-0002-1615-0009

David Uehling − *Ontario Institute for Cancer Research, Toronto, Ontario M5G 0A3, Canada;* orcid.org/0000-0002-9748-0500

Gennady Poda − *Department of Pharmaceutical Sciences, Leslie Dan Faculty of Pharmacy, University of Toronto, Toronto, Ontario M5S 3M2, Canada; Ontario Institute for Cancer Research, Toronto, Ontario M5G 0A3, Canada*

Henry Krause − *Donnelly Centre for Cellular and Biomolecular Research, University of Toronto, Toronto, Ontario M5S 3E1, Canada*

Complete contact information is available at: https://pubs.acs.org/10.1021/acs.jmedchem.1c01542

Author Contributions

○C.S., L.M., and T.A.M.F. contributed equally to this work.

Author Contributions

⊗C.L.C. and L.A.S.R. contributed equally to this work.

Funding

L.A.S.R. gratefully acknowledges support from National Council of Technological and Scientific Development (CNPq #310509/2011-4, #490203/2012-4, #3308486/2020-0). C.L.C. gratefully acknowledges support from NSERC RGPIN 03666-14 and the Canada−Israel Health Research Initiative, jointly funded by the Canadian Institutes of Health Research, the Israel Science Foundation, the International Development Research Centre Canada, and the Azreili Foundation (109155-001). L.M. was a recipient of a CGS-D fellowship from NSERC. C.S. is a recipient of a post-graduate scholarship from the Republic of Turkey. T.A.M.F. was a recipient of a fellowship from Coordenação de Aperfeiçoamento de Pessoal de Nível Superior—Brasil (CAPES) and CNPq (#490203/2012−4). G.P. acknowledges support from the Ontario Institute for Cancer Research and its funding from the Government of Ontario.

Notes

The authors declare the following competing financial interest(s): C.L.C., L.A.S.R., and L.M. are co-authors on a patent related to this work.

■ ABBREVIATIONS USED

CNSL, cashew nut shell liquid; DA, decanoic acid; HDL, high-density lipoprotein; IFD, induced-fit docking; LDL, low-density protein; MA, myristic acid; OA, oleic acid; PPAR, peroxisome proliferator-activated receptor; RXR, retinoid X receptor; RLU, relative luciferase units; SAR, structure−activity relationship; SPPARMs, selective PPAR modulators; SA, stearic acid; TZD, thiazolidinedione

■ REFERENCES

(1) Saklayen, M. G. The global epidemic of the metabolic syndrome. *Curr. Hypertens. Rep.* **2018**, *20*, No. 12.

(2) Nolan, P. B.; Carrick-Ranson, G.; Stinear, J. W.; Reading, S. A.; Dalleck, L. C. Prevalence of metabolic syndrome and metabolic syndrome components in young adults: A pooled analysis. *Prev. Med. Rep.* **2017**, *7*, 211−215.

(3) Sathyaprakash, R.; Henry, R. R. Preventing diabetes by treating aspects of the metabolic syndrome. *Curr. Diabetes Rep.* **2002**, *2*, 416−422.

(4) Haffner, S. M. Dyslipidemia management in adults with diabetes. *Diabetes Care* **2004**, *27*, S68−S71.

(5) Kahn, S. E.; Hull, R. L.; Utzschneider, K. M. Mechanisms linking obesity to insulin resistance and type 2 diabetes. *Nature* **2006**, *444*, 840−846.

(6) Ford, E. S.; Li, C.; Sattar, N. Metabolic syndrome and incident diabetes: Current state of the evidence. *Diabetes Care* **2008**, *31*, 1898−1904.

(7) Eckel, R. H.; Alberti, K. G.; Grundy, S. M.; Zimmet, P. Z. The metabolic syndrome. *Lancet* **2010**, *375*, 181−183.

(8) Evans, R. M.; Barish, G. D.; Wang, Y. X. Ppars and the complex journey to obesity. *Nat. Med.* **2004**, *10*, 355−361.

(9) Kersten, S.; Desvergne, B.; Wahli, W. Roles of ppars in health and disease. *Nature* **2000**, *405*, 421−424.

(10) Gronemeyer, H.; Gustafsson, J. A.; Laudet, V. Principles for modulation of the nuclear receptor superfamily. *Nat. Rev. Drug Discovery* **2004**, *3*, 950−964.

(11) Mangelsdorf, D. J.; Thummel, C.; Beato, M.; Herrlich, P.; Schutz, G.; Umesono, K.; Blumberg, B.; Kastner, P.; Mark, M.; Chambon, P.; Evans, R. M. The nuclear receptor superfamily: The second decade. *Cell* **1995**, *83*, 835−839.

(12) Kliewer, S. A.; Sundseth, S. S.; Jones, S. A.; Brown, P. J.; Wisely, G. B.; Koble, C. S.; Devchand, P.; Wahli, W.; Willson, T. M.; Lenhard, J. M.; Lehmann, J. M. Fatty acids and eicosanoids regulate gene expression through direct interactions with peroxisome proliferator-activated receptors alpha and gamma. *Proc. Natl. Acad. Sci. U.S.A.* **1997**, *94*, 4318−4323.

(13) Itoh, T.; Yamamoto, K. Peroxisome proliferator activated receptor gamma and oxidized docosahexaenoic acids as new class of ligand. *Naunyn-Schmiedeberg's Arch. Pharmacol.* **2008**, *377*, 541−547.

(14) Berger, J.; Moller, D. E. The mechanisms of action of ppars. *Annu. Rev. Med.* **2002**, *53*, 409−435.

(15) Lefebvre, P.; Chinetti, G.; Fruchart, J. C.; Staels, B. Sorting out the roles of ppar alpha in energy metabolism and vascular homeostasis. *J. Clin. Invest.* **2006**, *116*, 571−580.

(16) Ahmadian, M.; Suh, J. M.; Hah, N.; Liddle, C.; Atkins, A. R.; Downes, M.; Evans, R. M. Ppar gamma signaling and metabolism: The good, the bad and the future. *Nat. Med.* **2013**, *19*, 557−566.

(17) Wagner, K. D.; Wagner, N. Peroxisome proliferator-activated receptor beta/delta (pparbeta/delta) acts as regulator of metabolism linked to multiple cellular functions. *Pharmacol. Ther.* **2010**, *125*, 423−435.

(18) Wang, Y. X.; Zhang, C. L.; Yu, R. T.; Cho, H. K.; Nelson, M. C.; Bayuga-Ocampo, C. R.; Ham, J.; Kang, H.; Evans, R. M. Regulation of muscle fiber type and running endurance by ppardelta. *PLoS Biol.* **2004**, *2*, No. e294.

(19) Michalik, L.; Auwerx, J.; Berger, J. P.; Chatterjee, V. K.; Glass, C. K.; Gonzalez, F. J.; Grimaldi, P. A.; Kadowaki, T.; Lazar, M. A.; O'Rahilly, S.; Palmer, C. N.; Plutzky, J.; Reddy, J. K.; Spiegelman, B. M.; Staels, B.; Wahli, W. International union of pharmacology. Lxi. Peroxisome proliferator-activated receptors. *Pharmacol. Rev.* **2006**, *58*, 726−741.

(20) Fruchart, J. C. Peroxisome proliferator-activated receptor-alpha (pparalpha): At the crossroads of obesity, diabetes and cardiovascular disease. *Atherosclerosis* **2009**, *205*, 1−8.

(21) Jones, D. Potential remains for ppar-targeted drugs. *Nat. Rev. Drug Discovery* **2010**, *9*, 668−669.

(22) Wright, M. B.; Bortolini, M.; Tadayyon, M.; Bopst, M. Minireview: Challenges and opportunities in development of ppar agonists. *Mol. Endocrinol.* **2014**, *28*, 1756−1768.

(23) Hiukka, A.; Maranghi, M.; Matikainen, N.; Taskinen, M. R. Pparalpha: An emerging therapeutic target in diabetic microvascular damage. *Nat. Rev. Endocrinol.* **2010**, *6*, 454−463.

(24) Chatterjee, S.; Majumder, A.; Ray, S. Observational study of effects of saroglitazar on glycaemic and lipid parameters on indian patients with type 2 diabetes. *Sci. Rep.* **2015**, *5*, No. 7706.

(25) Gregoire, F. M.; Zhang, F.; Clarke, H. J.; Gustafson, T. A.; Sears, D. D.; Favelyukis, S.; Lenhard, J.; Rentzeperis, D.; Clemens, L. E.; Mu, Y.; Lavan, B. E. Mbx-102/jnj39659100, a novel peroxisome proliferator-activated receptor-ligand with weak transactivation activity retains antidiabetic properties in the absence of weight gain and edema. *Mol. Endocrinol.* **2009**, *23*, 975−988.

(26) Fukui, Y.; Masui, S.; Osada, S.; Umesono, K.; Motojima, K. A new thiazolidinedione, nc-2100, which is a weak ppar-gamma activator, exhibits potent antidiabetic effects and induces uncoupling protein 1 in white adipose tissue of kkay obese mice. *Diabetes* **2000**, *49*, 759−767.

(27) DePaoli, A. M.; Higgins, L. S.; Henry, R. R.; Mantzoros, C.; Dunn, F. L.; INT131-007 Study Group. Can a selective ppar gamma modulator improve glycemic control in patients with type 2 diabetes with fewer side effects compared with pioglitazone? *Diabetes Care* **2014**, *37*, 1918−1923.

(28) Choi, J. H.; Banks, A. S.; Estall, J. L.; Kajimura, S.; Bostrom, P.; Laznik, D.; Ruas, J. L.; Chalmers, M. J.; Kamenecka, T. M.; Bluher, M.; Griffin, P. R.; Spiegelman, B. M. Anti-diabetic drugs inhibit obesity-linked phosphorylation of ppargamma by cdk5. *Nature* **2010**, *466*, 451−456.

https://doi.org/10.1021/acs.jmedchem.1c01542
J. Med. Chem. 2022, 65, 1961−1978

(29) Lemes, L. F. N.; de Andrade Ramos, G.; de Oliveira, A. S.; da Silva, F. M. R.; de Castro Couto, G.; da Silva Boni, M.; Guimaraes, M. J. R.; Souza, I. N. O.; Bartolini, M.; Andrisano, V.; do Nascimento Nogueira, P. C.; Silveira, E. R.; Brand, G. D.; Soukup, O.; Korabecny, J.; Romeiro, N. C.; Castro, N. G.; Bolognesi, M. L.; Romeiro, L. A. S. Cardanol-derived ache inhibitors: Towards the development of dual binding derivatives for Alzheimer's disease. *Eur. J. Med. Chem.* **2016**, *108*, 687−700.
(30) Cerone, M.; Uliassi, E.; Prati, F.; Ebiloma, G. U.; Lemgruber, L.; Bergamini, C.; Watson, D. G.; Ferreira, T. d. A. M.; Roth Cardoso, G. S. H.; Soares Romeiro, L. A.; de Koning, H. P.; Bolognesi, M. L. Discovery of sustainable drugs for neglected tropical diseases: Cashew nut shell liquid (cnsl)-based hybrids target mitochondrial function and atp production in *Trypanosoma brucei*. *ChemMedChem* **2019**, *14*, 621−635.
(31) Rossi, M.; Freschi, M.; de Camargo Nascente, L.; Salerno, A.; de Melo Viana Teixeira, S.; Nachon, F.; Chantegreil, F.; Soukup, O.; Prchal, L.; Malaguti, M.; Bergamini, C.; Bartolini, M.; Angeloni, C.; Hrelia, S.; Soares Romeiro, L. A.; Bolognesi, M. L. Sustainable drug discovery of multi-target-directed ligands for Alzheimer's disease. *J. Med. Chem.* **2021**, *64*, 4972−4990.
(32) de Andrade Ramos, G.; Souza de Oliveira, A.; Bartolini, M.; Naldi, M.; Liparulo, I.; Bergamini, C.; Uliassi, E.; Wu, L.; Fraser, P. E.; Abreu, M.; Kiametis, A. S.; Gargano, R.; Silveira, E. R.; Brand, G. D.; Prchal, L.; Soukup, O.; Korábečný, J.; Bolognesi, M. L.; Soares Romeiro, L. A. Discovery of sustainable drugs for Alzheimer's disease: Cardanol-derived cholinesterase inhibitors with antioxidant and anti-amyloid properties. *RSC Med. Chem.* **2021**, *12*, 1154−1163.
(33) de Souza, M. Q.; Teotonio, I.; de Almeida, F. C.; Heyn, G. S.; Alves, P. S.; Romeiro, L. A. S.; Pratesi, R.; de Medeiros Nobrega, Y. K.; Pratesi, C. B. Molecular evaluation of anti-inflammatory activity of phenolic lipid extracted from cashew nut shell liquid (cnsl). *BMC Complementary Altern. Med.* **2018**, *18*, No. 181.
(34) Gomes Júnior, A. L.; Islam, M. T.; Nicolau, L. A. D.; de Souza, L. K. M.; Araujo, T. S. L.; Lopes de Oliveira, G. A.; de Melo Nogueira, K.; da Silva Lopes, L.; Medeiros, J. R.; Mubarak, M. S.; Melo-Cavalcante, A. A. C. Anti-inflammatory, antinociceptive, and antioxidant properties of anacardic acid in experimental models. *ACS Omega* **2020**, *5*, 19506−19515.
(35) Stasiuk, M.; Kozubek, A. Biological activity of phenolic lipids. *Cell. Mol. Life Sci.* **2010**, *67*, 841−860.
(36) Sung, B.; Pandey, M. K.; Ahn, K. S.; Yi, T.; Chaturvedi, M. M.; Liu, M.; Aggarwal, B. B. Anacardic acid (6-nonadecyl salicylic acid), an inhibitor of histone acetyltransferase, suppresses expression of nuclear factor-kappab-regulated gene products involved in cell survival, proliferation, invasion, and inflammation through inhibition of the inhibitory subunit of nuclear factor-kappabalpha kinase, leading to potentiation of apoptosis. *Blood* **2008**, *111*, 4880−4891.
(37) Uliassi, E.; de Oliveira, A. S.; de Camargo Nascente, L.; Romeiro, L. A. S.; Bolognesi, M. L. Cashew nut shell liquid (CNSL) as a source of drugs for Alzheimer's disease. *Molecules* **2021**, *26*, No. 5441.
(38) Proschak, E.; Heitel, P.; Kalinowsky, L.; Merk, D. Opportunities and challenges for fatty acid mimetics in drug discovery. *J. Med. Chem.* **2017**, *60*, 5235−5266.
(39) Tontonoz, P.; Hu, E.; Spiegelman, B. M. Stimulation of adipogenesis in fibroblasts by ppar gamma 2, a lipid-activated transcription factor. *Cell* **1994**, *79*, 1147−1156.
(40) Nesto, R. W.; Bell, D.; Bonow, R. O.; Fonseca, V.; Grundy, S. M.; Horton, E. S.; Le Winter, M.; Porte, D.; Semenkovich, C. F.; Smith, S.; Young, L. H.; Kahn, R. Thiazolidinedione use, fluid retention, and congestive heart failure. *Diabetes Care* **2004**, *27*, 256−263.
(41) Miyazaki, Y.; Mahankali, A.; Matsuda, M.; Mahankali, S.; Hardies, J.; Cusi, K.; Mandarino, L. J.; DeFronzo, R. A. Effect of pioglitazone on abdominal fat distribution and insulin sensitivity in type 2 diabetic patients. *J. Clin. Endocrinol. Metab.* **2002**, *87*, 2784−2791.
(42) Stern, J. H.; Rutkowski, J. M.; Scherer, P. E. Adiponectin, leptin, and fatty acids in the maintenance of metabolic homeostasis through adipose tissue crosstalk. *Cell Metab.* **2016**, *23*, 770−784.
(43) Maeda, N.; Takahashi, M.; Funahashi, T.; Kihara, S.; Nishizawa, H.; Kishida, K.; Nagaretani, H.; Matsuda, M.; Komuro, R.; Ouchi, N.; Kuriyama, H.; Hotta, K.; Nakamura, T.; Shimomura, I.; Matsuzawa, Y. Ppar gamma ligands increase expression and plasma concentrations of adiponectin, an adipose-derived protein. *Diabetes* **2001**, *50*, 2094−2099.
(44) Tiefenbach, J.; Moll, P. R.; Nelson, M. R.; Hu, C.; Baev, L.; Kislinger, T.; Krause, H. M. A live zebrafish-based screening system for human nuclear receptor ligand and cofactor discovery. *PLoS One* **2010**, *5*, No. e9797.
(45) Kamata, S.; Oyama, T.; Saito, K.; Honda, A.; Yamamoto, Y.; Suda, K.; Ishikawa, R.; Itoh, T.; Watanabe, Y.; Shibata, T.; Uchida, K.; Suematsu, M.; Ishii, I. Pparalpha ligand-binding domain structures with endogenous fatty acids and fibrates. *iScience* **2020**, *23*, No. 101727.
(46) Itoh, T.; Fairall, L.; Amin, K.; Inaba, Y.; Szanto, A.; Balint, B. L.; Nagy, L.; Yamamoto, K.; Schwabe, J. W. Structural basis for the activation of ppargamma by oxidized fatty acids. *Nat. Struct. Mol. Biol.* **2008**, *15*, 924−931.
(47) Shang, J.; Brust, R.; Griffin, P. R.; Kamenecka, T. M.; Kojetin, D. J. Quantitative structural assessment of graded receptor agonism. *Proc. Natl. Acad. Sci. U.S.A.* **2019**, *116*, 22179−22188.
(48) Yoshikawa, C.; Ishida, H.; Ohashi, N.; Itoh, T. Synthesis of a coumarin-based ppargamma fluorescence probe for competitive binding assay. *Int. J. Mol. Sci.* **2021**, *22*, No. 4034.
(49) Wu, C. C.; Baiga, T. J.; Downes, M.; La Clair, J. J.; Atkins, A. R.; Richard, S. B.; Fan, W.; Stockley-Noel, T. A.; Bowman, M. E.; Noel, J. P.; Evans, R. M. Structural basis for specific ligation of the peroxisome proliferator-activated receptor delta. *Proc. Natl. Acad. Sci. U.S.A.* **2017**, *114*, E2563−E2570.
(50) Patel, R.; Patel, M.; Tsai, R.; Lin, V.; Bookout, A. L.; Zhang, Y.; Magomedova, L.; Li, T.; Chan, J. F.; Budd, C.; Mangelsdorf, D. J.; Cummins, C. L. LXRβ is required for glucocorticoid-induced hyperglycemia and hepatosteatosis in mice. *J Clin Invest.* **2011**, *121*, 431−441.

https://doi.org/10.1021/acs.jmedchem.1c01542
J. Med. Chem. 2022, 65, 1961−1978